Dietary wheat amylase trypsin inhibitors worsen chronic liver disease in preclinical models of non-alcoholic fatty liver disease and liver fibrosis

A Thesis for the award of the degree of

DOCTOR OF NATURAL SCIENCES

Submitted to the

Faculty of Biology

Carried out in the Faculty of Medicine

Institute of Translational Immunology

Johannes Gutenberg-University Mainz

By

Muhammad Ashfaq Khan

Born in Peshawar, Pakistan

on 04.05.1988

Mainz, August 2018

Dean:

1. Reviewer:

2. Reviewer:

Day of defense:

Declaration

Muhammad Ashfaq Khan

Summary

A Westernized diet and sedentary life style are the main contributing factors triggering the onset of obesity and non-alcoholic fatty liver disease. However, general dietary components that have low nutritional value and have the potential to trigger inflammatory responses may also be of great importance. In this respect, a common dietary component, wheat amylase trypsin inhibitors (ATI) that have a negligible nutritional value were shown to activate intestinal macrophages and dendritic cells via toll like receptor 4. Importantly, once activated by nutritional ATI, these cells leave the gut to the surrounding mesenteric lymph nodes and likely other sites, potentially promoting intestinal as well as extra-intestinal inflammation. The liver is particularly prone to such effects, according to the postulated immunological gut-liver axis, with anticipated effects of such signals on the course of chronic liver disease, such as non-alcoholic fatty liver disease (NAFLD) and its severe form NASH (non-alcoholic steatohepatitis), and liver fibrosis in general. I therefore studied how far nutritional ATI may affect the severity of liver fibrosis and non-alcoholic fatty liver disease (NAFLD), obesity and the metabolic syndrome upon feeding mice with experimental liver fibrosis or NAFLD ATI-enriched vs ATI-free diets. For liver fibrosis, Mdr2-/- FVB mice that develop spontaneous secondary biliary fibrosis resembling human primary sclerosing cholangitis received a carbohydrate and protein (zein from corn) defined and vitamin/mineral/essential amino acid supplemented control diet, or 0.7% of the zein being replaced by purified ATI for 6 weeks. For NAFLD/NASH, male C57Bl6J mice received the zein-based diet with or without the carbohydrates replaced by 53% of calories by defined fats (high fat diet, HFD), with or without 30% of the zein being replaced by wheat gluten (G, containing about 0.15g ATI per 10g; HFD/G/ATI), or 0.7% of the zein being replaced by purified ATI (HFD/ATI) for 8 weeks. At sacrifice blood, liver and peripheral adipose tissues (in the NAFLD mice) were collected for biochemical, immunological and histological analysis. In the NAFLD mice, insulin resistance (IR) was assessed by an intraperitoneal glucose tolerance test (IPGTT). Mice on the high fat diet (HFD) gained significant weight and developed IR. Compared to the HFD alone, mice fed the HFD/G/ATI, or the HFD/ATI diets dose-dependently gained significantly more weight and displayed significantly higher serum transaminases and triglycerides, epididymal, mesenteric and inguinal fat, and a higher insulin resistance. ATI feeding induced enhanced liver and adipose tissue inflammation, with an increased M1-type macrophage polarization and infiltration, and a

significantly increased fibrogenic response in the liver compared to HFD mice on the ATI-free diet. Mdr2-/- mice on the ATI containing diet developed a significantly more severe liver fibrosis than their ATI-free controls. Therefore, in mice wheat ATI when ingested in quantities comparable to human average consumption exacerbate all features of NAFLD/NASH, the metabolic syndrome and biliary fibrosis despite their irrelevant caloric value. These findings underline the detrimental effects of wheat ATI on ongoing peripheral chronic diseases, especially liver inflammation and fibrosis, and NAFLD/NASH related adipose tissue inflammation and insulin resistance. They are currently tested in clinical studies, also in view of consumption and finally the production of healthier (ATI-reduced wheat) products.

Zusammenfassung

Eine verwestlichte Ernährung und eine sitzende Lebensweise sind die Hauptfaktoren, die die Entstehung von Fettleibigkeit und nicht-alkoholischer Fettleber auslösen. Jedoch könnten auch allgemeine diätetische Komponenten, die einen geringen Nährwert haben und potentiell Entzündungsreaktionen auslösen, von großer Wichtigkeit sein. In dieser Hinsicht wurde gezeigt, dass eine übliche Diätkomponente, Weizen-Amylase-Trypsin-Inhibitoren (ATI), die einen vernachlässigbaren Nährwert haben, intestinale Makrophagen und dendritische Zellen über Toll-like-Rezeptor 4 aktivieren. Wichtig ist, dass diese Zellen, sobald sie durch die ATI-Ernährung aktiviert werden, den Darm zu den umgebenden mesenterischen Lymphknoten und wahrscheinlich anderen Organen verlassen, was nach bisherigen Daten sowohl die intestinale als auch die extraintestinale Entzündung fördert. Die Leber ist gemäß der postulierten immunologischen Darm-Leber-Achse besonders anfällig für solche Effekte, wobei die erwarteten Auswirkungen solcher Signale auf den Verlauf einer chronischen Lebererkrankung wie der nichtalkoholischen Fettlebererkrankung (NAFLD) und ihrer schweren Form NASH (nicht-alkoholische Steatohepatitis) und ggf. auch die Leberfibrose im Allgemeinen verhältnismässig ausgeprägt sein sollten. Ich untersuchte daher, wie weit ATI in der Nahrung den Schweregrad der Leberfibrose und der nicht-alkoholischen Fettlebererkrankung (NAFLD), von Fettleibigkeit und des metabolischen Syndroms bei in Mäusen mit experimenteller Leberfibrose oder NAFLD beeinflussen können. Mdr2-/- FVB-Mäuse, die eine spontane sekundäre biliäre Fibrose ähnlich der humanen primär sklerosierenden Cholangitis entwickelen, erhielten eine Kontrolldiät aus definierten Kohlenhydraten und Protein (Zein aus Mais), ergänzt mit Vitaminen/Mineralstoffen und essentiellen Aminosäure oder die gleiche Diät, in der 0,7% des Zeins durch gereinigte ATI ersetzt wurden, für 6 Wochen. Im Modell der NAFLD/NASH erhielten männliche C57Bl6J-Mäuse die zeinbasierte Diät mit oder ohne Ersatz von der Kohlenhydrate durch 53% der Kalorien an definierten Fetten (Hochfettdiät, HFD). Ferner wurden in weiteren Gruppen 30% des Zeins durch Weizengluten (G, enthaltend etwa 0,15 g ATI pro 10 g; HFD/G/ATI), oder 0,7% des Zeins durch gereinigte ATI ersetzt(HFD/ATI) . Die Diäten erfolgten über 8 Wochen ersetzt. Zum Versuchsende wurden Blut, Leber und peripheres Fettgewebe für biochemische, immunologische und histologische Analysen gesammelt. In den NAFLD-Mäusen wurde ferner die Insulinresistenz (IR) durch einen intraperitonealen Glucosetoleranztest (IPGTT) gemessen. Die NAFLD-Mäuse nahmen signifikant an

Gewicht zu und entwickelten eine IR. Im Vergleich zur HFD alleine nahmen Mäuse, welche die HFD/ G /ATI oder HFD / ATI-Futter dosisabhängig erhielten, signifikant mehr Gewicht und zeigten signifikant höhere Serumtransaminasen und Triglyceride, Epididymal--, Mesenterial- und Leistenfett und eine höhere Insulinresistenz. ATI-Fütterung induzierte eine verstärkte Leber- und Fettgewebsentzündung mit einer vermehrten Makrophagenpolarisation und -infiltration vom M1-Typ und einer signifikant erhöhten fibrogenen Reaktion in der Leber im Vergleich zu HFD-Mäusen unter der ATI-freien Diät. Mdr2 - / - Mäuse auf der ATI-haltigen Diät entwickelten eine signifikant schwerere Leberfibrose als ihre ATI-freien Kontrollen. Daher verschlimmern mit der Diät aufgenommene Weizen ATI in Mengen, die mit dem menschlichen Durchschnittsverbrauch vergleichbar sind, alle Merkmale der NAFLD, des metabolischen Syndroms und der biöiären Leberfibrose, trotz ihres irrelevanten Kalorienwerts. Diese Ergebnisse unterstreichen die schädlichen Auswirkungen von Weizen-ATI auf anhaltende periphere chronische Erkrankungen, insbesondere Leberentzündung und Fibrose, und die mit NAFLD/NASH verbundene Fettgewebeentzündung und Insulinresistenz. Die Ergebnisse werden z.Zt in klinischen Studien überprüft, u.a. in Hinblick auf den Verzehr und schließlich die Produktion gesünderer (ATI-reduzierter Weizen-) Produkte.

Abbreviations used

ATI	amylase trypsin inhibitors
TLR-4	toll like receptor 4
NAFLD	non-alcoholic fatty liver disease
IPGTT	intra peritoneal glucose tolerance test
CLS	crown like structures
MetS	metabolic syndrome
T2D	type 2 diabetes
IR	insulin resistance
HFD/G/ATI	high fat diet mixed with gluten (with ATI)
HFD/ATI	high fat diet mixed with wheat amylase trypsin inhibitors
NASH	non-alcoholic steatohepatitis
HCC	hepatocellular carcinoma
HFD	high fat diet
ALT	alanine aminotransferase
Arg1	arginase 1
α-SMA	alpha-smooth muscle actin
COL1α1	procollagen α1 (I)
DCs	dendritic cells
ECM	extracellular matrix
HSC	hepatic stellate cell
Hyp	hydroxyproline
IL-1β	interleukin-1β
MMP	matrix metalloprotease
mRNA	messenger RNA
NAS	NAFLD activity score

qPCR	quantitative real-time PCR
TGFβ1	transforming growth factor beta 1
TIMP-1	tissue inhibitor of metalloproteinases-1
TNFα	tumor necrosis factor α
Ym1	beta-N-acetylhexosaminidase

Units

%	percent
°C	degree centigrade
d	day
dl	0.1 liter
g	gram
h	hour
min	min
mg	milligrams
mm	millimeter
µg	micrograms
µm	micrometer
U/L	units per liter

Table of Contents

1. Introduction

1.1 The epidemiology of NAFLD and NASH

The epidemic of nonalcoholic fatty liver disease (NALFD) and its severe, inflammatory form, nonalcoholic steatohepatitis (NASH) is primarily due to convergent factors that have taken roots in modern or developing societies. This epidemic is largely due to overeating, unhealthy foods and a sedentary lifestyles.[1] NAFLD present with a wide spectrum of disease severity, including the extremes of mere non-alcoholic fatty liver (NAFL) and NASH that can progress to cirrhosis and lead to primary hepatocellular carcinoma (HCC).[2] NASH associated cirrhosis or HCC is currently becoming the leading cause of liver related morbidity and mortality and except for rigorous life-style changes that – as in obesity – are difficult to achieve – and liver transplantation for end-stage NAFLD, effective pharmacological therapy is still in development.[3-6] NAFLD is also associated with various extrahepatic cancers, e.g. colorectal cancer in males and females, and breast cancer in females.[7] The numerous epidemiological studies on NAFLD and NASH prevalence and incidence show heterogeneity due to difficulties for an exact diagnosis and assessment of severity which are currently based on liver biopsy, ultrasonography, magnetic resonance imaging, combined with blood tests such as liver enzymes.[3] The overall collective prevalence worldwide is about 25% based on the published literature between 1989 and 2015 as diagnosed by ultrasound imaging, with most dramatic increases in South America and the Middle East.[8] Moreover, Male gender, age, obesity, insulin resistance and cardiovascular complications that are associated with the metabolic syndrome are central risk factors for NAFLD. In obese and type 2 diabetic/prediabetic individuals, the prevalence of NAFLD is about 30-50% and 80-90%, respectively reaching up to 90% when patients have also developed hyperlipidemia. In addition, in children, NAFLD prevalence is about 3-10% with 40-70% among obese children. Though the incidence and natural history of NAFLD are difficult to determine on a broad scale, the disease is tightly linked, but only partly overlapping with obesity, a Western "fast food" diet, lack of physical exercise (sedentary lifestyle), explaining the continuous rise of NASH/NAFLD in Western and developing countries.[9]

1.5 Pathogenesis

The spectrum of nonalcoholic fatty liver disease (NAFLD) ranges from mere steatosis (excess triacylglycerol deposition in >5% of hepatocytes) to steatosis with inflammation, steatosis with hepatocellular ballooning degeneration, both features of nonalcoholic steatohepatitis (NASH that are usually associated with fibrosis, and finally progression to cirrhosis, in the absence of excessive alcohol consumption as causative factor (<30 g per day for men and <20 g per day for women).[10] Features of the metabolic syndrome, including obesity, insulin resistance (IR), type 2 diabetes mellitus (T2DM), dyslipidemia and hypertension are linked to NAFLD which can be considered as the hepatic manifestation of the metabolic syndrome.[11, 12]

In addition to the conventional two hit hypotheses that postulates that apart from liver fat accumulation a defined second pathology is necessary to drive the progression of NAFLD to NASH and fibrosis/cirrhosis, the pathogenesis and progression of NAFLD/NASH should be considered as a stepwise accumulation of these abnormalities involving several fundamental biochemical, metabolic and immunological processes.[1, 13]

Hepatocyte toxicity, specifically lipoapoptosis, is triggered when the restorative mechanisms to control the toxic effects of free fatty acids (FFA) and their oxidative by-products accumulate in the liver as a result of the generation of excess reactive oxygen species (ROS), endoplasmatic reticulum (ER) stress, mitochondrial and finally hepatocellular dysfunction. This hepatocellular damage stimulates a cascade of immune-mediated events that further aggravate hepatocellular injury and both necrotic and apoptotic cell death pathways; once these events continue or even worsen in a vicious cycle, the liver scar producing cells (hepatic stellate cells and myofibroblasts) become activated and fibrosis progression (fibrogenesis) occurs.[14] The basic pathogenic events occurring in NASH and fibrosis that also involve the gut-liver axis are schematically shown in **Fig. 1**.

In addition to established co-factors of liver and adipose tissue inflammation, the intestine is emerging as a new site for immunologic changes that affect all organs of the body, but especially the liver as first major organ being supplied by vessels emanating from the intestine[15]. In line with this, there are multiple independent modifiers of health as well as risk factors of disease, especially those related to the intestinal microbiome[16] and dietary factors that themselves shape the composition of the microbiome and/or the intestinal immune system.[15] To deal with the rising tide of the NAFLD disease

spectrum, and apart from central life style changes such as preventing overnutrition and doing more physical exercise, several promising novel therapeutic targets, including specific (micro-) nutrients, are emerging that may help to curb the NAFLD/NASH epidemic or support the treatment of existing disease.[17, 18]
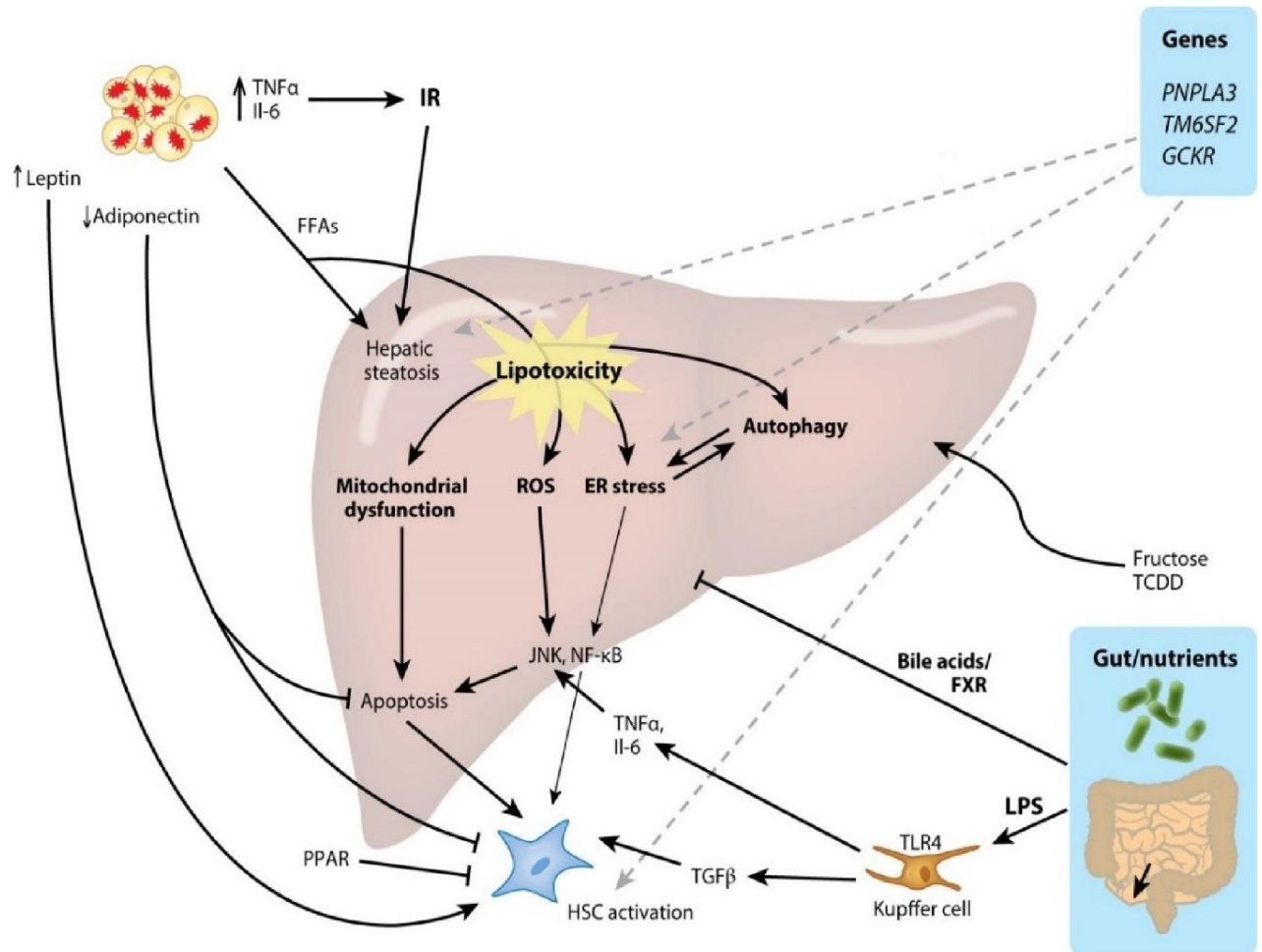
Fig.1 Simplified scheme of the interplay between different pathogenic processes during the evolution of nonalcoholic steatohepatitis that finally lead to hepatic stellate cell (HSC) activation and fibrogenesis (adopted from [16])

1.2 Histological characterization of NAFLD/NASH

Assessment of liver steatosis by ultrasound can be used as a crude method to screen for NAFLD, but for the exact diagnosis of NAFLD the activity of the disease, extent and location of fibrosis, including liver architectural remodeling (fibrosis stage), liver biopsy is still the widely used "gold standard.[19] Proven noninvasive tests for detection of all features of NAFLD, especially the extent of fibrosis or the activity of fibrogenesis or fibrolysis are lacking in the clinic, although recent developments are encouraging as regards refined magnetic resonance imaging and especially noninvasive serum markers of liver fibrosis and fibrogenesis. [1, 20-23]

1.2.1 Hepatic steatosis

Retention of triglycerides in the diseased liver in the form of macrovesicular and to a lesser degree microvesicular droplets within hepatocytes is the major feature of NAFLD.[24] Histological assessment of steatosis is graded as the percentage of steatotic hepatocytes (0–33%, 33–66%, or >66%) in the liver parenchyma and remains the most reproducible quantitative method[25]. However, MR imaging is becoming the prime noninvasive quantification method for liver fat. In adults, fat accumulation starts in the perivenular zone 3 or the liver acinus[22] whereas in children it often starts in the periportal area.[24]

1.2.2 Histological and inflammatory features of steatohepatitis

Composite features of accumulation of fat, ballooning of hepatocytes and intra-acinar (lobular inflammation) occurring in zone 3 in the presence or absence of fibrosis is the main diagnostic criteria for NASH. Moreover, during the progression of fibrosis and tissue remodeling, the active inflammatory NASH lesions may lose strict acinar localization.[24]

Hepatocyte injury is due to lipoapoptosis, with hepatocyte apoptotic bodies and lytic necrosis, and ballooning in its most characteristic advanced form. Ballooned hepatocytes have the characteristics of a balloon like shape as being enlarged and swollen and have a condensed and abnormal distribution of keratins 8 and 18 within the hepatocytes.[26]

Intra-acinar (lobular) inflammatory foci harbor mixed inflammatory cells including lymphocytes, macrophages, neutrophils and sometimes eosinophils. In addition, the extent of portal inflammation in NASH also varies and is linked to the escalation of disease activity, and increases with the severity of insulin resistance, excess free fatty

acids, ROS and toxic lipid products, both in pediatric and adult patients.[27] In adults, fibrosis starts perisinusoidally and is localized in zone 3 followed by bridging fibrosis and finally cirrhosis.[28]

1.3 Histological grading of NAFLD disease activity and staging of fibrosis

Brunt et al.,[28] devised a semiquantitative grading and staging system for NASH and fibrosis respectively (**Table.1**), including the location of fibrosis. The grading components of the score are a composite to assess disease activity and comprise steatosis (fat accumulation), inflammation and ballooning. Kleiner et al., refined this score by better quantifying disease severity using these 3 categories and fibrosis, the NAS score [25] (**Table. 2**). Fibrosis is scored from stage 0-4, with zone 3 perisinusoidal (stage 1), portal (stage 2), bridging (stage 3) and cirrhosis (stage 4).[28] In clinical trials and in medical practice, a NAS>5 (earlier also NAS>4) has been used to diagnose NASH.

Table. 1 The system for grading and staging of steatohepatitis by Brunt et al. [28]

	Grade of steatohepatitis				Staging of Fibrosis	
Grade	**steatosis**	**Ballooning**	**Lobular inflamm.**	**Portal inflamm.**	**stage**	**Fibrosis**
Mild	Involves up to 2/3rds	Occasional zone 3	Scattered mild acute and chronic	None or mild	0	none
Moderate	Any degree	Obvious, zone 3	Mild to moderate	Mild to moderate	1	Zone 3 perisinusoidal fibrosis only
Severe	Typically, more than 2/3rd	Marked, mainly zone 3	Moderate to severe, associated with ballooning	Moderate to severe	2	Zone 3 perisinusoidal fibrosis and periportal fibrosis
					3	Bridging fibrosis
					4	cirrhosis

Table 2 The scoring system of Kleiner et al. [4]

Feature	Definition	Score
❖ Steatosis	<5%	0
	5-33%	1
	33-66%	2
	>66%	3
❖ Lobular inflammation	No foci	0
	<2 foci per 20x field	1
	2-4 foci per 20x field	2
	>4 foci per 20x field	3
❖ Hepatocyte ballooning	No ballooning	0
	Few (<3) ballooned cells	1
	Many (>3) ballooned cells	2

1.4 Murine models of NAFLD

Various murine models have been developed to help elucidate the pathogenesis of NAFLD and NASH. Selective and context specific models are also being employed to test novel therapeutic approaches to treat NASH and fibrosis. These models have been recently reviewed as to their ability to reflect human NASH and to predict the efficacy of interventions and pharmacological therapies.[29,30] In the following, a selection of frequently used and especially of preclinical useful NAFLD/NASH models, omitting most of those that rely on genetic mutations that rarely occur or have not been demonstrated in man.

1.4.1 ob/ob mouse

ob/ob mice are leptin-deficient due to a spontaneous mutation in the leptin gene causing them to overeat and become obese and thereby develop hepatic steatosis[31]. However, these mice do not develop steatohepatitis and usually require a second hit to progress towards steatohepatitis.[32] The main limitations of this model are therefore[33]

1. Lack of progression towards hepatic fibrosis - however this model is suitable to study transition of steatosis towards steatohepatitis.
2. The ob gene mutations is very rare in humans and leptin levels in humans do not correlate well with NASH severity.

1.4.2 db/db Mouse

db/db mice develop a similar phenotype as ob/ob mice because of a dysfunctional mutation in the leptin receptor, while having normal leptin levels.[34] These animals develop a mild pathology comparable to the ob/ob mice. The same limitations apply as to the ob/ob mice.

1.4.3 High Fat Diet

The proximate diet composition of high fat diet and selection of rodent (rat vs mice) are the main drivers in developing features of the NASH phenotype e.g. a variant of HFD (71% fat, 11% carbohydrate and 18% protein) develops NASH features in rat after 3 weeks.[35] Moreover, addition of fructose to high fat diet such as ALIOS or western diet (high fructose and high Trans-fat diets) display features of NASH.[36]

1.4.4 High-cholesterol (and high fat) diet

A cholesterol-rich atherogenic diet induces steatosis, inflammation and fibrosis over a period of usually 16-24 weeks, with an even more severe phenotype when 60% of calories is added e.g. as cocoa butter.[37] Accumulation of free cholesterol has been

shown in severe NASH phenotype confirming a contributory role of cholesterol in development of NAFLD and NASH.[38] However, the cholesterol that needs to be given is excessive (1-2% in weight of the diet) that is 50-100 fold more than in the human nutrition. Moreover, the predominant phenotype is severe atherosclerosis, which is not necessarily seen in NASH.

1.4.5 Methionine- and choline-deficient (MCD) diet

The MCD diet has been widely used model to study the lipoapoptotic damage to hepatocytes that is an important feature of NASH.[16] These mice also develop a (relative, per g of liver tissue) increase in fibrosis with steatosis and severe steatohepatitis.[39] The main disadvantage of this model is the lack of other central pathogenic mechanisms of the metabolic syndrome, especially of insulin resistance that is a key feature of human NAFLD and NASH. Moreover, mice on the MCD diet lose significant body weight (up to 50% of the initial body weight) contrary to human NAFLD/NASH where patients are usually obese.

1.4.6 Choline-deficient L-amino acid–defined (CDAA) diet

The CDAA diet causes a pathology closely resembling human NAFLD/NASH while retaining some features of the MCD model (severe hepatic lipoaptosis and inflammation). Importantly, mice do gain weight when on a high fat diet, develop insulin resistance and fibrosis. Currently, this model is preferred by us and increasingly used by other research groups.

1.5 Liver fibrosis and primary sclerosing cholangitis

Despite of liver transplantation, currently no treatment option is available to reverse and/or stop the progression of primary sclerosing cholangitis (PSC) to cirrhosis.[1, 40] PSC is an autoimmune disease with environmental cofactors, especially bacterial translocation from the gut into the liver and into bile ducts, and occurs prominently in male patients with ulcerative colitis. It is a progressive cholesteric liver disease bile ductular inflammatory infiltrates, periductular progressive fibrosisis, with frequent obstructions of smaller (intrahepatic) and larger (extraheptic) bile ducts and a high risk of hepato- and cholangiocellular carcinoma.[41, 42] Proliferating bile ductular structures that are often dysfunctional drive the surrounding fibrogenic response via activation of the surrounding portal firboblasts and hepatic stellate cells resulting in increasing deposition of extracellular matrix, i.e., scar tissue[43]. The term "ductular reaction" is preferred over ductular proliferation due to the fact that this phenomenon occurs in association with others cells that include infiltrating immune cells, bone marrow derived

macrophages, recruited T cells, fibroblastic and resident inflammatory cells.[44] Mdr2-/-FVB mice spontaneously develop a fibrotic and later neoplastic liver disease resembling human PSC.[43] In this model, the canalicular phospholipid transporter of hepatocytes/cholangiocytes that is the product of the *Mdr2* (*Abcb4*) gene and that is the orthologue of human *MDR3* (*ABCB4*)[45] is deleted resulting in the spontaneous development of sclerosing cholangitis[46] and cholelithiasis[47] induced by the loss of phosphatidylcholine from bile and the inability to excrete toxic bile acids into bile.[48] The accumulating toxic bile acids are important drivers of hepatocyte damage and finally inflammation and fibrosis, as in the rare human genetic disease "progressive familiar intrahepatic cholestasis type 3" (PFIC-3) where functional MDR3 is lacking[49]. Notably, enhanced activation of the innate immune system via toll-like receptor (TLR) signalling, especially via TLR4, has been implicated in all types of chronic fibrotic liver diseases. [50, 51] Important TLR ligands are microbial DNA (TLR9), RNA (TLR3), cell wall glycans (TLR2), and particularly lipopolysacchardide (LPS, TLR4), stressing the role of certain microbial pathogens in liver disease severity and progression.[52] Importantly, we previously identified and characterized an important nutritional activator of TLR4 in the intestine, wheat amylase trypsin inhibitors (ATI, see below).[53]

1.6 The gut-liver axis

The importance of the gut-liver axis is increasingly recognized due to promising results of therapeutic and disease preventive approaches. This area of research is continuously expanding but requires further mechanistic studies to translate into clinical practice.[54] There are increasing data showing that the gut-liver axis plays an important role in the pathogenesis of metabolic liver disorders because the liver (in addition to the intestine) acts as the first line of defense against gut-derived antigens.[55] In this vein, the liver receives 70% of its antigen rich blood from the gastrointestinal tract [56] and 30% of the whole blood volume passes through the liver every minute.[57] In addition, increased intestinal permeability is implicated in the transfer of endotoxins and (micro-) nutrients into the portal circulation and liver where these molecules can contribute a cascade of necro-inflammation in NASH.[58] Importantly, immune cells that emanate from the gut may also affect liver inflammation in NASH and other fibrotic liver diseases.[59] While the effect of certain gut microbiota and microbiota-derived products, mainly lipopolysaccharide had been implicated in NASH pathogenesis. A specific disease promoting effect of dietary protein on NASH pathogenesis has never been reported.[17, 18] Thus, diet and/or other gut-derived products, as well as inflammatory cells activated

in the intestine may affect the liver. In the gut, pathogen or damage-associated molecular patterns (PAMPs or DAMPs) which may cross the dysfunctional permeability barrier of gut may be operative. This will subsequently activate liver innate immune directly or indirectly (via emigration of activated immune cells from the gut to the liver) and trigger (enhanced) necroinflammation and fibrosis as a "second hit", e.g. in the transition from simple fatty liver (a benign stage) to NASH.[60, 61] A simplified illustration of these events is shown in **Fig. 2**.
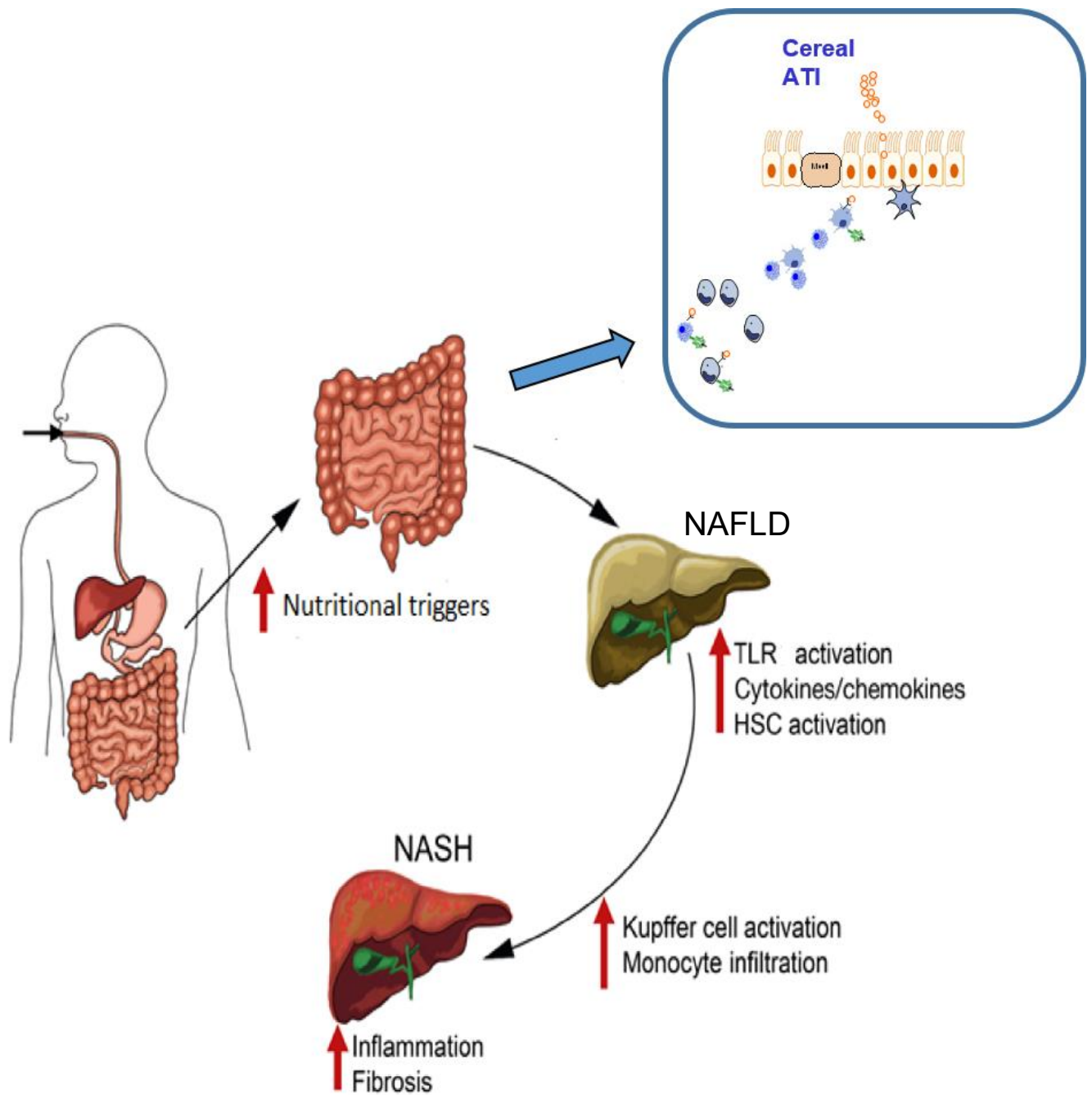
Fig. 2 Simplified illustration of the gut-liver-axis in modifying (promoting) NALFD/NASH (modified from).[62] Proinflammatory factors stemming from the intestine either directly or via exit of activated gut immune cells to the liver enhance the already pre-existing inflammation thereby promoting NASH with subsequent fibrosis.

1. 1.7 Wheat amylase trypsin inhibitors (ATI)

Wheat amylase trypsin inhibitors are a class of no-gluten proteins in wheat grains representing 2-4% of wheat protein (compared to 85-90% for the gluten proteins). They belong to the largely water soluble albumin fraction of wheat proteins and their major roles appear to confer some resistance to pests and especially to regulate the availability of glucose from the storage carbohydrate starch and of amino acids from the gluten storage proteins during the germination process.[63] Wheat ATI are highly resistant to gastrointestinal proteases due to a highly compact disulfide-linked compact structures.[17, 53, 64] There are theoretically (based on genetic analysis) up to 17 different ATI, with high secondary structure homology. Based on their electrophoretic mobilities and solubilities in buffers, these ATI can be classified into three subfamilies of approximately 50–60, 24–30, and 12–15 kDa that form non-covalent associations of tetra, di and monomers, respectively. The major tetrameric AtI are the CM class, mainly CM3, the major dimers are 0.19, 0.28 and 0.53 that also exist as monomers.[64-66,63, 67, 68] Importantly, the major ATI in wheat, CM3 and 0.19 that represent >50% of ATI in most wheats stimulate TLR4 on myeloid cells, prominently (intestinal) macrophages and dendritic cells after oral ingestion.[17, 53] Here, they do not only enhance intestinal inflammatory diseases but also inhalative and food allergies, and likely other extraintestinal chronic diseases.[69-72] The hypothetical but already partly demonstrated pathway of inflammatory signal transduction from the gut to the periphery is illustrated in **Fig.3**.
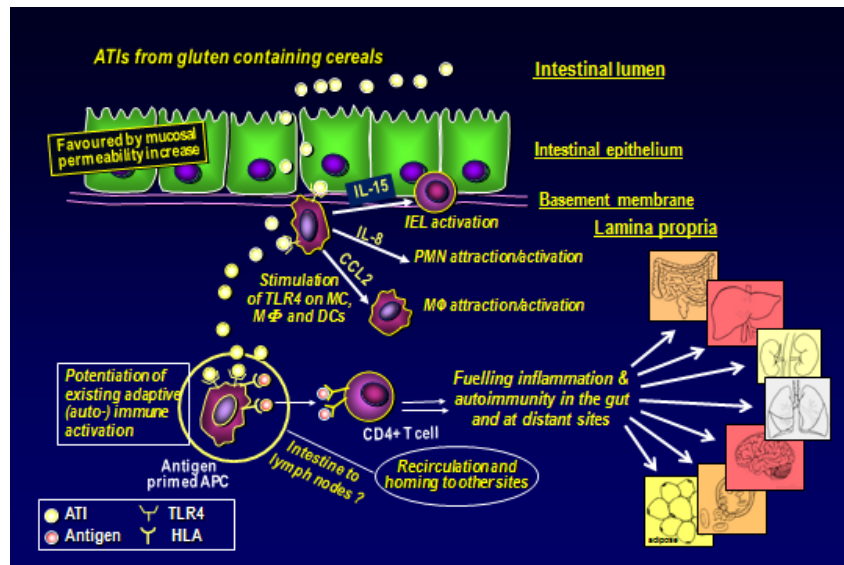
Fig. 3 ATI survive intestinal degradation and trigger intestinal mucosal myeloid innate immune cell activation via TLR4 signaling. Once activated, these cells largely leave the gut towards surrounding lymph nodes and possibly peripheral organs. There, they contact between ATI-activated antigen presenting cells (APC) and already existing antigen-specific specific T cells that are present and circulate in e.g. autoimmune diseases, where the ATI-activated APC further stimulate ongoing T cell immunity, thus fueling pre-existent (autoimmune) diseases. DC, dendritic cell; IEL, intraepithelial lymphocyte; HLA, human lymphocyte antigen; MC, monocyte; MΦ, macrophage,(Adopted from [70])

1.9 Purpose of this thesis

Microbiota associated TLR4 signalling has been postulated as important driver of NASH and fibrosis. Recently identified nutritional activators of TLR4 are the "wheat amylase trypsin inhibitors" (ATI). While ATI-mediated TLR4 signals have been shown to be propagated from the intestine to the periphery, so far their role in chronic liver disease pathogenies in general and in the pathogenesis of NALFD/NASH in particular has not been investigated. ATI represent 3% of wheat protein, the most common staple food worldwide. ATI are highly resistant to digestive proteolysis and activate intestinal innate immunity via toll like receptor 4 (TLR4) on monocytes, macrophages and dendritic cells that can leave the gut to transmit signals to other organs, especially the liver. Therefore, the purpose of this thesis was to assess the effect of nutritional ATI equivalent in quantity to human average wheat ingestion on the severity of diet induced NAFLD and adipose tissue inflammation in mice. Moreover, the effect of dietary ATI in the Mdr2 knockout mouse model of primary sclerosing cholangitis was tested to evaluate if dietary ATI affect liver fibrosis progression in general.

2. Materials and methods

2.1 Materials

2.1.1 Instruments used in carrying out the scientific work in the present thesis

Name	Manufacturer
Balance Sartorius AX2202	PK Electronic Ettlingen, Germany
Balance Sartorius AX124	PK Electronic Ettlingen, Germany
Bio-Rad T100™ thermal cycler	Bio-Rad, München, Germany
Bio Rad Powerpac basic	Bio-Rad, München, Germany
Bio Rad Powerpac HC	Bio-Rad, München, Germany
Centrifuge HeraeusFresco21	Thermoscientific, Schwerte, Germany
Centrifuge 5804R	Eppendorf, Hamburg, Germany
Centrifuge VWR mini star	VWR International, Darmstadt, Germany
ChemiDoc™ XRS+ System	Bio Rad, München, Germany
Ergone Pipette 1000ul	Starlab GmbH, Hamburg, Germany
Ergone Pipette 200ul	Starlab GmbH, Hamburg, Germany
Ergone Pipette 20ul	Starlab GmbH, Hamburg, Germany
Ergone Pipette 10ul	Starlab GmbH, Hamburg, Germany
Ergone Pipette 2,5ul	Starlab GmbH, Hamburg, Germany
Eppendorf centrifuge 5804R	Eppendorf, Hamburg, Germany
Eppendorf centrifuge 5415R	Eppendorf, Hamburg, Germany
FACS Canto II	BD Biosciences, Heidelberg, Germany
Gentle MACS Dissociator 3013	MACS Miltenybiotec
HeraeusMultifuge X3R centrifuge	Thermoscientific, Schwerte, Germany
HXP120C kublercodix	Carl Zeiss, München, Germany
Leica EG 1150c	Leica, Wetzlar, Germany
Leica TP1020	Leica, Wetzlar, Germany
Leica CM1950	Leica, Wetzlar, Germany
Microtome Leica RM2255	Leica, Wetzlar, Germany
Microtome Leica HI1210	Leica, Wetzlar, Germany
Microtome blade MX 35 premier34°/80mm	Thermoscientific, Schwerte, Germany
MulticalPH meter pH 538	WTW, Weilheim, Germany
Rocking platform	VWR International, Darmstadt, Germany
Rotamax 120	Heidolph Instruments, Schwabach, Germany
TECAN hydrospeed	Tecan, Männedorf, Germany
TECAN infinite M 200Pro	Tecan, Männedorf, Germany
Zeiss microscope AX10	Carl Zeiss, München, Germany

2.1.2 Consumables

Name	Manufacturer
1000μl Tips	Starlab GmbH, Ahrensburg, Germany
200μl Tips	Starlab GmbH, Ahrensburg, Germany
0,1-20μl GradanteTips	Starlab GmbH, Ahrensburg, Germany
96 well plates flat bottomed	Greiner Bio-One, Frickenhausen, Germany
96-well fast thermal cycling	Life technologies GmbH, Darmstadt, Germany
MicroAmp optical adhesive film	Life technologies GmbH, Darmstadt, Germany
Cellstar tubes (15ml and 50ml)	Greiner Bio-One, Frickenhausen, Germany
Cell strainer (100μm)	BD Bioscience, Heidelberg, Germany
Cryo tubes	Greiner Bio-One, Frickenhausen, Germany
DAKO Pen	Dako Deutschland GmbH, Hamburg, Germany
Disposal bags	Carl Roth, Karlsruhe, Germany
Disposal base molds	Simport, Beloeil, Canada
FACS tubes, polystyrene, 5 ml	BD Biosciences, Heidelberg, Germany
Filter paper	Whatman, Dassel, Germany
Gentle MACS C tubes	Miltenyi Biotec, Bergisch-Gladbach, Germany
Histosette tissue processing/embedding cassettes	Simport, Hague, The Netherlands
Inject-F (single use injection) 1ml	B.Braun, Melsungen, Germany
Knittel glass cover slips 24*50mm	Iss, Bradford, United Kingdom
Microscope coverslips	Life technologies GmbH, Darmstadt, Germany
PCR tubes 0.2 ml Flat cap	Greiner Bio-One, Fricken hausen, Germany
Polysine slides	Thermo scientific, Braunschweig, Germany
Superfrost ultra plus slides	Thermo scientific, Braunschweig, Germany
Safe-lock tubes 2.0 ml	Eppendorf, Hamburg, Germany
Safe-lock tubes 1.5 ml	Eppendorf, Hamburg, Germany
Serological pipette, sterile (5,10,25 ml)	Greiner Bio-One, Frickenhausen, Germany
Super frost ultraplus slides	Thermoscientific, Braunschweig, Germany

2.1.3 Reagents and kits

Name	Manufacturer
1-Propanol pure	Applichem, Darmstadt, Germany
2-Propanol pure	Applichem, Darmstadt, Germany
70% Ethanol	Carl Roth GmbH, Karlsruhe, Germany
Ammonium Persulfate	Sigma Aldrich, Steinheim, Germany
Antibody diluent	Dako Deutschland GmbH, Hamburg, Germany
Bovine serum albumin(BSA)	Sigma Aldrich, Steinheim, Germany
cDNA SuperMix reverse transcription kit	Quanta, Gaithersburg, USA
Chloroform	Applichem, Darmstadt, Germany
Collagenase from Clostridium histolyticum	Sigma Aldrich, Steinheim, Germany
Direct RED 80	Sigma Aldrich, Steinheim, Germany
DAB Peroxidase (HRP) Substrate Kit	Vector Laboratories, Inc., Burlingame, USA
DEPC treated water	Life technologies GmbH, Darmstadt, Germany
DNase I	Sigma Aldrich, Steinheim, Germany
Ethanol absolute	VWR chemicals, Fontenay-sous-bois, France
Ethylendiamintetraacetatic acid (EDTA)	Sigma Aldrich, Steinheim, Germany
Eosin	Carl Roth GmbH, Karlsruhe, Germany
FACS-Clean	BD Bioscience, Heidelberg, Germany
FACS- Flow	BD Bioscience, Heidelberg, Germany
FACS-Rinse	BD Bioscience, Heidelberg, Germany
Fetal calf serum(FCS)	Invitrogen, San Diego, USA
Formaldehyde 4%	Carl Roth GmbH, Karlsruhe, Germany
Glycerol minimum 99%	Sigma Aldrich, Steinheim, Germany
Hematoxylin	Merck, Darmstadt, Germany
Horse serum	Vector Laboratories, Inc., Burlingame, USA
Hydrochloric acid 6N	VWR, Darmstadt, Germany
Hydrogen peroxide 30%	Carl Roth GmbH, Karlsruhe, Germany
Ketamin Hameln 50mg/ml	Hameln pharmaceuticals, Hameln, Germany
L-Hydroxyproline	Merck KGaA, Hessen, Germany
Methanol Technical grade	Applichem, Darmstadt, Germany
Potassium dihydrogen phosphate	Carl Roth GmbH, Karlsruhe, Germany

Picric acid	Sigma Aldrich, Steinheim, Germany
Protease inhibitor	Roche, Mannheim, Germany
Potassium chloride	Carl Roth GmbH, Karlsruhe, Germany
Potassium phosphate monobasic	Sigma Aldrich, Steinheim, Germany
qScript cDNA SuperMix	VWR(Quantabio) Darmstadt, Germany
Rompun 2%	Bayer vital GmbH, Leverkusen, Germany
Roti-Histokitt II	Carl Roth, Karlsruhe, Germany
Sodium chloride	Carl Roth GmbH, Karlsruhe, Germany
Sodium phosphate dibasic	Carl Roth GmbH, Karlsruhe, Germany
Sodium citrate dihydrate	Fisher- scientific New Jersey, USA
Sodium dodecyl sulfate	Sigma Aldrich, Steinheim, Germany
Sudan III	Sigma Aldrich, Steinheim, Germany
SYBR Green PCR mix	Life technologies GmbH, Darmstadt, Germany
Taqman master mix	Life technologies GmbH, Darmstadt, Germany
Triton^{TM} X-100	Sigma Aldrich, Steinheim, Germany
Trizma base	Sigma Aldrich, Steinheim, Germany
Ribozol	Ampresco, Solon, USA
Tween 20	Merck KGaA, Darmstadt, Germany
VECTASTAIN ABC Systems	Vector Laboratories, Inc., Burlingame, USA
Xylene	Applichem, Darmstadt, Germany
β-mercapthoethanol	Sigma Aldrich, Steinheim, Germany

2.1.4 Antibodies

Name	Manufacturer
anti α-SMA (clone: E184)	Abcam plc, Cambridge, United Kingdom
anti CD11b (clone: M1/70)	Biolegend, Fell, Germany
anti CD11c (clone: N418)	Biolegend, Fell, Germany
anti CD45(clone: 30-F11)	Biolegend, Fell, Germany
anti CD68(clone: FA-11)	Biozol Diagnostica Vertrieb GmbH, Eching, Germany
anti F4/80(clone: BM8)	Biolegend, Fell, Germany
anti Ly6c(clone: HK1.4)	Biolegend, Fell, Germany
anti Ym1(clone: 01404)	Stem cell Technologies, Köln, Germany
Biotinylated goat anti rabbit IgG (H+L) (BA-1000)	Vector Laboratories, Inc., Burlingame, USA
Biotinylated goat anti rat IgG (H+L) (BA-9400)	Vector Laboratories, Inc., Burlingame, USA
Goat anti rabbit IgG-HRP(sc-2004)	Santa Cruz Biotechnology Inc., Santa Cruz, USA

2.1.5 General buffers and solutions

Acidified water	Glacial acetic acid 5ml dd H_2O 1000 ml
Antigen unmasking citrate buffer	Na-sodium citrate 10mM (pH 6.0)
Blocking solution	2 to 5% normal donkey or Goat serum
Citric acetate buffer	5% citric acid (5 g) 7.24% sodium acetate (7.24 g) 3.4% sodium hydroxide (NaOH 3.4 g) 1.2% glacial acetic acid (1.2 ml) dissolved in 100 ml dH_2O, adjusted to pH 6.0
Chloramine T	32 ml citric acetate buffer pH 6.0 4 ml distilled water 4 ml n-propanol 564 mg chloramine T hydrate heated to 50°C to dissolve
Ehrlich's reagent	7.9 ml n-propanol 3.31 ml 70% perchloric acid 1.91 mg 4-Dimethylaminobenzaldehyde prepared freshly before the experiment.
FACS fixation buffer	0.1 % formaldehyde in PBS
Phosphate buffered saline(PBS) 10X stock solution	137 mM sodium chloride (NaCl 80 g) 2.0 mM potassium chloride (KCl 2 g) 1.8 mM monopotassium phosphate (KH_2PO_4 2.4 g) to 1 L dH_2O adjust pH to 7.4 with hydrochloric acid (HCl)
Tris buffered saline (TBS) 10X stock solution	24,2 g Trizma base ($C4H11NO3$) 80 g sodium chloride (NaCl) to 1l Adjusted to pH 7.6 with HCl
PBST 1X	100 ml 10X PBS stock solution 900 ml d H_2O, 1 ml Tween 20
TBST 1X	100 ml 10X TBS stock solution 900 ml d H_2O, 1 ml Tween 20
Ammonium persulfate (APS) 10%(w/v)	10 g APS in 100 ml d H_2O
Blocking buffer	1X TBST with 5% w/v nonfat dry milk
Tris-glycine 10X stock solution	121 g Trizma base glycine 577 g dissolved in 4 L d H_2O
Primary antibody dilution buffer	1X TBST with 5% BSA or 5% nonfat dry milk
Sodium dodecyl sulfate10%	10 g SDS into 100ml d H_2O
Transfer Buffer	100 ml 10X Tris-Glycine buffer 200 ml methanol 700 ml dH_2O
0.1% Sirius Red solution	Sirius Red 0.5 g saturated picric acid 500 ml

2.1.6 Quantitative real time PCR (qPCR) primer for marker analysis

Target gene	Forward primer (5'-3')	Taqman Probe	Reverse primer (5'-3')
TGFß1	AGAGGTCACCCGCGTGC TAA	ACCGCAACAACGCCATCT ATGAGAAAACCA	TCCCGAATGTCTGACGT ATTGA
TIMP-1	TCCTCTTGTTGCTATCAC TGATAGCTT	TTCTGCAACTCGGACCTG GTCATAAGG	CGCTGGTATAAGGTGGTCTCGTT
MMP-2	CCGAGGACTATGACCGGGATAA	TCTGCCCCGAGACCGCTATGTCCA	CTTGTTGCCCAGGAAAGTGAAG
MMP-3	GATGAACGATGGACAGA GGATG	TGGTACCAACCTATTCCTGGTTGCTGC	AGGGAGTGGCCAAGTTCATG
MMP-9	CAGGATAAACTGTATGGCTTCTGC	CTACCCGAGTGGACGCGACCGT	GCCGAGTTGCCCCCA
MMP-13	GGAAGACCCTCTTCTTCTCT	TCTGGTTAACATCATCATAACTCCACACGT	TCATAGACAGCATCTACTTTGTT
TNFα	CTCAGCCTCTTCTCATTC	CACCACGCTCTTCTGTCTACTGA	GCCATAGAACTGATGAGA
Arg1 (SRBY)	GGTCCAGAAGAATGGAAGAGTCAG		CAGATATGCAGGGAGTCACC
CD68 (SRBY)	CTTCCCACAGGCAGCACAG		AATGATGAGAGGCAGCAAGAG
GAPDH	AGGTCGGTGTGAACGGATTTG		GGGGTCGTTGATGGCAACA

2.1.7 Diet formula

Ingredients	Low fat zein diet	High fat zein based diet	High fat with 30% wheat Gluten in zein based diet	High fat with 0.15% purified ATI in zein based diet
Zein (%)	22.100	22.100	15.470	21.6
Wheat gluten (%)	----	----	6.630	---
Purified wheat amylase trypsin inhibitors	---	---	---	0.7
Corn starch (pre-gelatinized) (%)	50.000	13.600	14.200	13.600
Maltodextrin (%)	5.000	5.000	5.000	5.000
Sucrose (%)	5.000	12.00	12.00	12.00
Cellulose (%)	5.200	7.700	7.700	7.700
DL-Methionine (%)	0.100	0.100	0.100	0.100
L-Cystine (%)	0.200	0.200	0.100	0.200
Vitamin Premix (%)	1.000	1.000	1.000	1.000
Mineral&trace elements premix (%)	6.000	6.000	6.000	6.000
Choline chorlide (%)	0.200	0.200	0.200	0.200
L-lysine HCl (%)	1.800	1.800	1.800	1.800
L-threonine (%)	0.300	0.300	0.180	0.300
L-tryptophan (%)	0.230	0.230	0.180	0.230
L-valine (%)	0.970	0.970	0.800	0.970
L-isoleucine	0.300	0.300	0.250	0.300
L-arginine, free base (%)	0.300	0.300	0.210	0.300
L-histindine, free base (%)	0.100	0.100	0.050	0.100
Cholesterol (%)	0.100	0.100	0.100	0.100
Soybean oil (%)	5.300	0	0	0
Corn oil (%)		28.000	28.000	28.000

2.2 Methods

2.2.1 Experimental animals

Animal experiments were approved by the State of Rhineland-Palatinate and performed in accordance with institutional and legal guidelines of the ethical committee of the Government of Rhineland Palatinate under the reference number 2317707/G12-1-007. Mice were age matched and were maintained in a temperature and light (12:12h: light:dark) controlled facility and had access to food and water *ad libitum*

ATI purification and bioactivity determination

ATI were purified to >70% by quantitative extraction of wheat flour using 50 mM ammonium bicarbonate, pH 7.8, and fractional precipitation with ammonium sulfate as described[53]. Gluten was purchased from Sigma (Lot#SLBD0196V). TLR4 stimulating bioactivity of purified ATI and of ATI in gluten was determined by a THP1 macrophage bioassay using IL-8 secretion as readout and transformed into μg of bioactive ATI. The amount of ATI subspecies (mainly dimeric 0.19 and tetrameric CM3) was confirmed by mass spectrometry. [53]

2.2.2. Diet preparations and feeding period

8-week-old male C57BL/6 mice were fed a basal carbohydrate and protein defined diet (22.1% of weight as the zein, the non-inflammatory protein from corn whose components otherwise show similarities to those of wheat, supplemented with amino acids, vitamins and minerals, combined with a low or high fat content (13 KJ% vs 53KJ% of calories as saturated fats) Apart from the low fat diet (LFD) and high fat diet (HFD) alone, groups of mice received these diets with 30% of the zein being isocalorically replaced by crude wheat gluten (which contains 1.5% ATI) or with 0.7% of the zein being replaced by purified ATI (**Table 1**). Thus, groups of 7-10 mice were kept on the following diets for 8 weeks: 1. Low fat diet (LFD) 2. High fat diet (HFD) 3. HFD with gluten that contains ATI (HFD/G/ATI) 4. HFD with purified ATI (HFD/ATI). During the feeding period, diet consumption and body weight were monitored thrice weekly. In the final 8 weeks of feeding, fasting blood samples were obtained from the tail vein for intraperitoneal glucose tolerance test (IPGTT). For liver fibrosis studies, age matched 6 weeks male Mdr2-/- FVB mouse were fed two different diets namely 1. Zein diet (ZD) and 2. Zein diet with purified ATI (ZD/ATI) for an additional 6 weeks. Prior to sacrifice, mice were anesthetized by intraperitoneal injection of a mixture of 100 mg ketamin/kg and 16 mg xylazin/kg for sacrifice and blood collection via cardiac

puncture. The liver, mesenteric, epididymal and inguinal adipose tissues were weighed and equal parts of liver and epididymal adipose tissue were fixed in OCT media (Medite, Burgdorf, Germany), in neutral-buffered formalin, or snap frozen in liquid nitrogen and kept at -80°C.

2.2.3 Routine blood analyses

Serum alanine aminotransferase (ALT) and serum triglycerides were determined by the Central Laboratory of the University Medical Centre Mainz according to standardized and regularly validated criteria.

2.2.4 Intraperitoneal glucose tolerance test (IPGTT)

The IPGTT test was performed as described.[73] Briefly, immediately before sacrifice mice were transferred to clean cages without access to food but with drinking water ad libitum for 8-10 h. Then a 20% solution of 2g glucose/kg of body weight was injected intraperitoneally. Blood samples were drawn from the tail vein immediately before and 15, 30, 60, and 120 min after the glucose challenge.

2.2.5 Evaluation of liver injury

Liver sections (7 µm) were fixed in tissue tek (SAKURA, The Netherlands) that provide optimum cutting temperature (OCT) and stained with Sudan III (Sigma, Steinheim, Germany). Liver 7µm cryosections were air dried at room temperature for 5 to 10 min and incubated in 0.3% Sudan III in 70% ethanol for 30 min, rinsed in distilled water and stained with hematoxylin for 3 min. After washing in distilled water, the stained sections were mounted with glycerol resinous medium and viewed in a Zeiss Axio Imager AX10 microscope with the suitable 400 power field. A series of random pictures covering most of the total tissue sections were generated, and Image J software was used to quantify liver fat. Paraffin-embedded liver sections (4 µm) were stained with haematoxylin and eosin (H&E, Sigma, Steinheim, Germany) and scored for liver inflammation and hepatocyte ballooning according to the NAS score[25] adapted for mouse liver.[74]

2.2.5.1 Hepatic collagen content determination

For hydroxyproline content determination biochemically, two different snap-frozen liver pieces (150–160 mg each) were hydrolyzed in 6N HCl at 110°C for 16 hours. Hydroxyproline standards (Merck), hydrolysate samples and blanks all in triplicate (5 µl per well) were added into a 96 well plates. 50 µl citrate-acetate buffer (Fisher-scientific) and 100 µl chloramine T (Sigma) solutions were added respectively to the hydrolyzed samples and hydroxyproline standards in the 96 well plates. After a 30-

min incubation on an orbital shaker at room temperature, a solution containing of 4-dimethylaminobenzaldehyde (Sigma), dissolved in 70% perchloric acid (Sigma) and 1-isopropanol (Applichem) were added to the samples and standards and after 5-min, pre-incubation absorbance of the solutions was measured before incubating the samples for 30 minutes at 65°C. The absorbance of the solutions in 96 well plates was measured at 550 nm wavelength (as post–incubation) and the levels of Hyp per milligram of liver tissue were calorimetrically quantified and calculated using the standard curve of a serial dilution of L-Hyp (Merck). Total hydroxyproline (mg/whole liver) were determined by multiplying the above determined liver weights with the relative hepatic Hyp concentration as described previously.[75]

2.2.5.2 Hematoxylin and eosin (H&E) staining

Briefly, paraffin embedded liver and epididymal sections were deparaffinized in xylene (three times for 5-min each) followed by steps washing in isopropyl alcohol 100% (two times for 3-min each) and subsequently dipped in descending concentration of isopropyl alcohol 95% and 70% for 3-min each and hydrated with distilled water for 5 minutes. After deparaffinization and hydration step, the tissue sections were immersed in hematoxylin for 2-3 min and washed in running water for 10 min to remove excess hematoxylin. The tissue sections were counter stained with eosin for up to 30 sec. For dehydration the tissues sections were immersed in ascending concentrations of isopropyl-alcohol solutions (70%, 95%, 95%, 100% and 100%) before washing the dipping in xylene (two times for 5 min each). H&E stained sections were mounted with resinous medium in the fume hood and properly covered and visualized in a Zeiss Axio Imager AX10 Microscope with the appropriate filters. Representative images were taken with an AxioCamMRc 5 camera where a minimum of 10 random high-power fields were taken and analyzed for all tissue sections. Quantitative analysis was performed using the Image J software (National Institute of Health, Bethesda, Maryland, USA).

2.2.5.3 Sirius red for collagen staining in liver

Paraffin embedded tissue sections were dewaxed, rinsed and hydrated twice for 5-min distilled water. Then, the tissue sections were incubated in 0.1% Sirius red in saturated picric acid solutions for 45 min and washed twice in 0.05% acetic acid (5 min). After this, tissue sections were washed in distilled water followed by dehydration step in ascending concentrations of isopropyl alcohol (70%, 95%, 100%) and finally two 5 min immersion in xylene. Slides with SR stained sections

were mounted with resinous medium in the fume hood and properly covered and visualized in a Zeiss Axio Imager AX10 Microscope with the appropriate filters. Representative images were taken with an AxioCamMRc 5 camera where a minimum of 10 random high-power fields were taken and analyzed for all tissue sections. Quantitative analysis was performed using the Image J software (National Institute of Health, Bethesda, Maryland, USA).

2.2.5.4 Sudan III staining for hepatic lipid content

Cryopreserved tissue sections were air dried at room temperature for 5 to 10 min. and then incubated in 0.3% Sudan III (prepared in 70% ethanol) for 30 min. After this, the samples were rinsed in distilled water and stained with hematoxylin for 3 to 5 min followed by washing step in tap water for 10 min to get rid of excess hematoxylin. Finally, the Sudan III stained sections were mounted with resinous medium and viewed in a Zeiss Axio Imager AX10 microscope with the suitable filters. Representative images were taken with an AxioCamMRc 5 camera using a Zeiss Axio Imager AX10 Microscope with the appropriate filters, stained tissue sections were visualized and a series of random pictures covering most of the total tissue sections were generated. The Image J software was employed to quantify images

2.2.5.5 Immunohistochemical staining and morphometry

Formalin fixed, paraffin embedded tissue sections were dewaxed, rehydrated and rinsed in water before proceeded to the antigen unmasking step. Tissue sections were boiled in 10 mM in sodium citrate buffer (pH 6.0) for 30 min to expose the target antigen. To avoid background due to endogenous peroxidase, tissue sections were incubated in 3% H_2O_2 10 min in deionized water. After this, sections were rinsed in distilled water and then incubated with 5% normal donkey serum for 30 to 45 min. Primary antibodies solutions were prepared using the antibodies e.g. anti-CD68 (1:100, Biozol, clone: FA-11), anti-Ym1 (1:500, Stemcell, clone: 01404) and anti-α-SMA (1:500, Abcam, clone: E184) and incubated overnight at 4°C. Next morning, the tissue sections were washed thrice in TBS buffer before incubating with respective biotinylated secondary antibody (1:500, Vector Labs, BA-1000) for 30 minutes at room temperature. To amplify the target antigen signal, tissue sections were incubated for additional 30 min with Avidin-Biotin complex at room temperature using the Vectastain ABC kit (Vector Laboratories) followed by colorimetric detecting via the DAB substrate kit (Vector Laboratories) and finally counterstained with hematoxylin. Using a Zeiss Axio Imager AX10 Microscope with the appropriate filters,

stained tissue sections were visualized and a series of random pictures covering most of the total tissue sections were generated. The Image J software were deployed to quantify.

Immunofluorescence staining and morphometry

Frozen intestinal 7μm sections from the terminal ileum were formalin fixed for 5 to 10 minutes. Tissue was blocked with 5% normal donkey serum and subsequently incubated with primary antibodies of anti-CD68 (1:100, Biozol, clone: FA-11), CD86 (1:100, Abcam, cat no: ab119857) and MHC-II (1:100, Abcam, cat no: 180779) for 2 hrs at room temperature and finally incubated with respective alexa-flour 488 labelled secondary antibodies. Stained intestinal sections were visualized and a series of random pictures were taken using a Zeiss Axio Imager AX10 Microscope with the appropriate magnification field (40x) and analyzed with Image J software.

2.2.5.6 Quantitative analysis of gene expression

After homogenizing the small pieces of tissues, following solubilization with Trizol (Invitrogen), phase separation was carried out by the addition of chloroform where RNA is in the upper aqueous phase, protein is the organic phase and DNA remains in the interface. After total RNA extraction, cDNA was prepared using iScript TMcDNA Synthesis kit (Quantum Bio). Primers used were either designed using the Primer Express software (Perkin Elmer, Foster City, CA) or previously used by others in published work as summarized in section 2.1.6**.** A&B step one plus real time PCR thermocycler (Applied Biosystems) machine were used for running qPCR reaction. The transcription levels of GAPDH were used to normalize the mRNA expression level of the target gene using the relative standard curve method (Sequence Detection Systems software version 2.2.2, Applied Biosystems).

2.2.5.7 Immune sub set analysis via flow cytometry

Liver tissues were homogenized with the gentleMACS dissociator (MACS Miltenyi Biotec, Germany) and incubated with 0.4% collagenase IV (Sigma), 1.6 nM DNaseI (Applichem) in 154 mM NaCl, 5.6 mM KCl, 5.5 mM glucose, 20.1 mM HEPES, 25 mM NaHCO$_3$, 2 mM CaCl$_2$, 2 mM MgCl$_2$, pH7.4, for 30 min at 37°C. Tissue homogenates were filtered through a 100 μm cell strainer (BD Bioscience, city, country) and centrifuged at 21xg for 4 min to remove contaminating hepatocytes. The supernatant was centrifuged at 300xg for 10 min and the pellet resuspended in red blood cells lysis solution (Ebioscience) for 10 min at RT and centrifuged for 10 min at 300g. Non-specific antibody binding sites were blocked with anti-Fc receptor IgG

(1:100, BD Bioscience, clone: 2.4G2) for 10 min, followed by centrifugation and subsequent incubation of the pellet with target FACS antibodies to CD45 (1:100, clone:30-F11), CD11b (1:100, clone: M1/70), Ly6C (1:100, clone: HK1.4) and F4/80 (1:100, clone: BM8). After antibody staining, cells were fixed with 1% formaldehyde buffer. Data were acquired on a FACS Canto II (BD Bioscience) and analyzed using the FlowJo 7.6 software (TreeSta).

2.2.6 Data analysis

Data were analyzed using Graphpad Prism 5.0 (GraphPad software, La Jolla, USA). Binary comparisons were done with the unpaired t test, and ANOVA was employed for multiple group comparisons. The data were expressed as the mean and standard error of the mean. Differences between groups with $p < 0.05$ were considered significant.

3. Results

3.1 Wheat amylase trypsin inhibitors promote murine obesity, inflammation and fibrogenesis in a murine model of non alcoholic steatohepatitis

3.1.1 ATI alone and in a gluten matrix promote body gain and insulin resistance

Mice were subjected to a short term high fat diet (HFD, 8 weeks) with amino acid supplemented zein from corn as defined, non-inflammatory protein component. Subgroups received a low fat diet (LFD) or the HFD, either with 30% of the zein being isocalorically replaced by gluten (which contains 1.5% as ATI, resulting in 0.45% of the zein as ATI; HFD/G/ATI), or with 0.7% of purified ATI as shown in the experimental scheme (HFD/ATI) **(Fig. 4)**. This amount of ATI compares well with the average human consumption, which is around 150 g of processed wheat flower per day in the normal Western or middle eastern diet.[12]

Mice fed the ATI containing HFD gained significantly more body weight than their controls on the HFD alone (**Fig. 5A-B**). Moreover, the HFD/ATI fed mice developed a graver insulin resistance (IR) than mice on the HFD alone **(Fig. 5C-D)**. Notably, the strongest effect was observed in mice that consumed the higher amount of purified ATI (0.7% of total protein) compared to mice that consumed 0.45% ATI, despite the massive consumption of gluten in the latter group (30% of total protein). In addition to this, ATI fed group has significantly higher serum triglycerides and ALT levels compare to controls (**Fig. 5, E-F**). This confirms our prior data that it is the TLR4 activating ATI and not the prevalent gluten proteins in wheat that stimulate innate immune cells and thus promote inflammation.[17, 18]
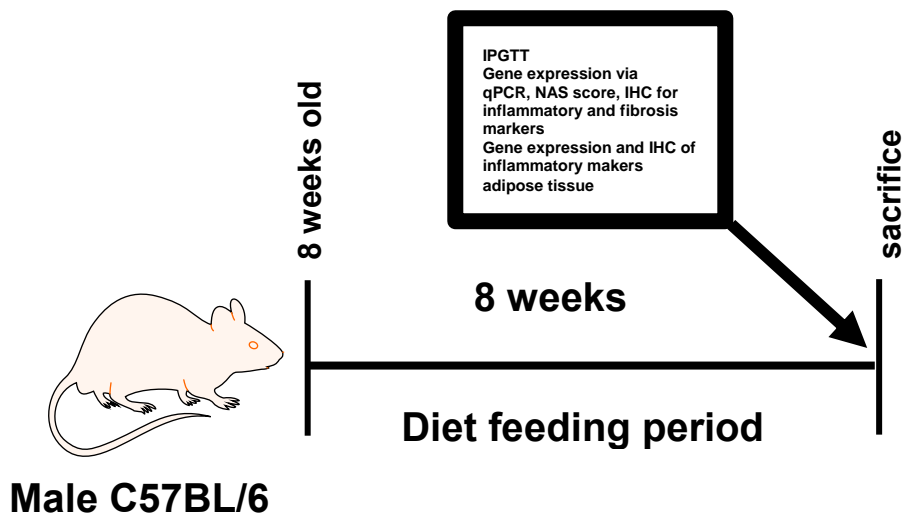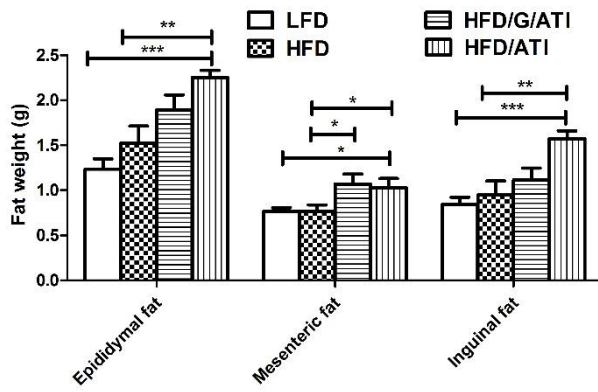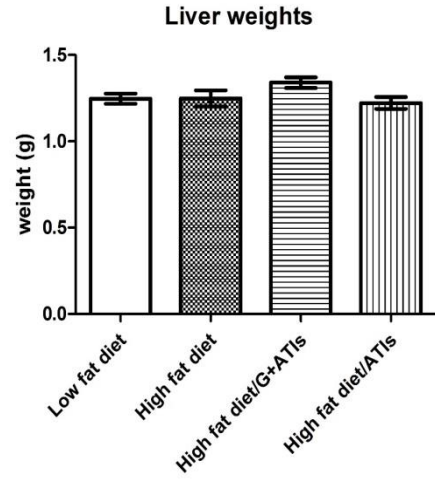
Fig.4 Experimental scheme. Age matched, 8 weeks old male C57BL/6 mice were fed experimental diets for 8 weeks, Intraperitoneal glucose tolerance test (IPGTT) and further indicated organ and plasma readouts were carried out at the end of the experimental period
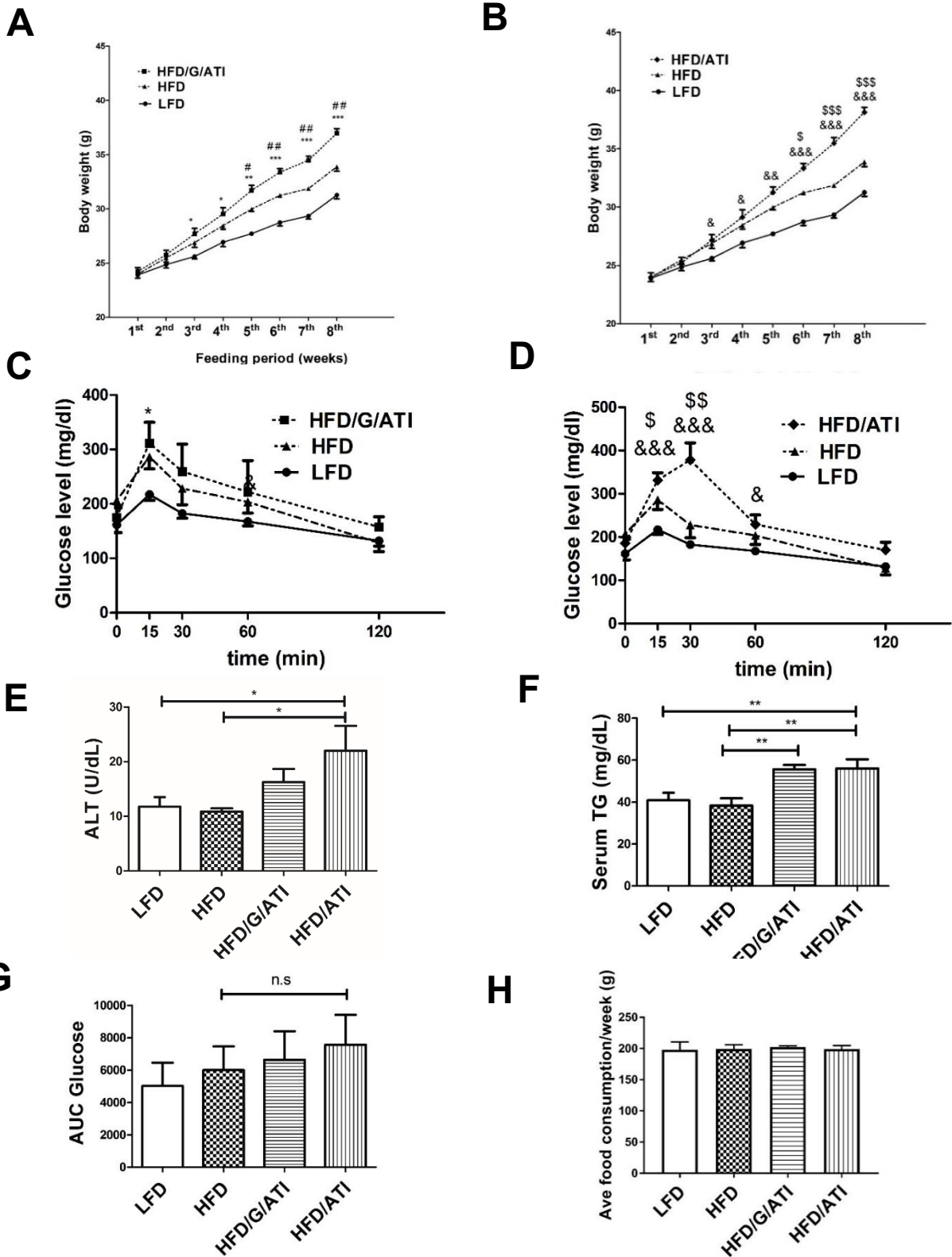
Fig.5 Accelerated weight gain and enhanced insulin resistance in mice fed ATI. Age matched wildtype mice were fed four different diets for 8 weeks. Body weight change over time: (A) low fat diet (LFD), high fat diet (HFD), HFD/G/ATI (G, 30% of protein as gluten, and 0.45% as ATI) and HFD/ATI (0.7% of protein as ATI). (B) Intraperitoneal glucose tolerance test (IPGTT) in the same dietary groups as shown in A. (C) Average area under the curve of the aforementioned groups. (D) Serum ALT (E) Serum triglycerides. (F) Average food consumption per week. Comparisons by ANOVA; data are means ± SEM for 7-10 mice per group; *$p<0.05$, **$p<0.01$, ***$p <0.001$ (HFD/G/ATI vs HFD); $^{\$}p<0.05$, $^{\$\$}p<0.01$ $^{\$\$\$}p<0.001$ (HFD/ATI vs HFD).

3.1.2 Correlation studies between mesenteric fat and epidydimal fat

This was paralleled by a significant accumulation of mesenteric, inguinal and epididymal fat **(Fig. 6A)**. There was a good correlation between the weights of mesenteric and epididymal adipose tissue in all groups except for a lack of significance in the HFD/G/ATI fed group **(Fig. 6C)**.
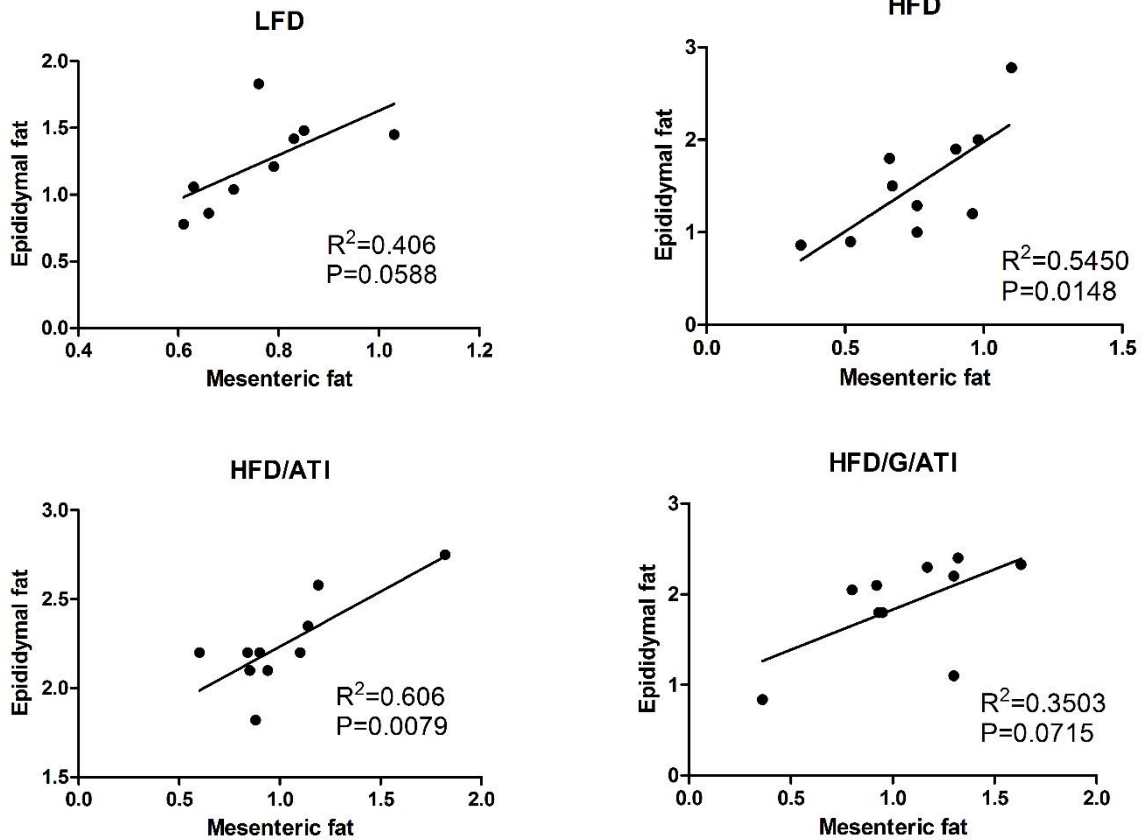
Fig.6 Increased expansion of central fat depots in mice fed ATI (A) Epididymal, mesenteric and inguinal adipose tissue weights in ATI-fed mice. (B) Liver weights (C) Correlation between mesenteric and epididymal fat mass between groups. Comparisons by ANOVA; data are expressed as means ± SEM for 7-10 mice per group; *$p<0.05$, **$p<0.01$, ***$p<0.001$.

### 3.1.3 Dietary ATI fuel adipose tissue inflammation

Compared to the HFD alone control group, mice fed the HFD/ATI or HFD/G/ATI diet showed worsened adipose tissue inflammation markers as revealed by gene expression of cd68, Il6 and Il1β (**Fig.7D**). Furthermore, the HFD/ATI and the HFD/G/ATI fed mice had enlarged adipocytes in addition to a significant increase in density of CD68+ (macrophage containing) crown like structures (CLSs) [76] compare to mice fed the HFD alone **(Fig. 7A-C)**.

3.1.4 ATI alone and in a gluten matrix worsen hepatic steatosis

There were pronounced hepatic steatosis in the HFD/ATI fed mice (with an increasing trend in the HFD/G/ATI group) compared to mice on the HFD alone as quantified by histological assessment using the criteria of the NAS score[25] (adopted for mouse livers) as detailed previously **(Fig. 8A-C)**. In addition to this, there were significant increase of hepatic lipid content in the HFD/ATI fed mice and an increased trend in the HFD/G/ATI fed group compared to mice on the HFD alone as demonstrated on Sudan III stained liver sections **(Fig. 8D**, **E)**.
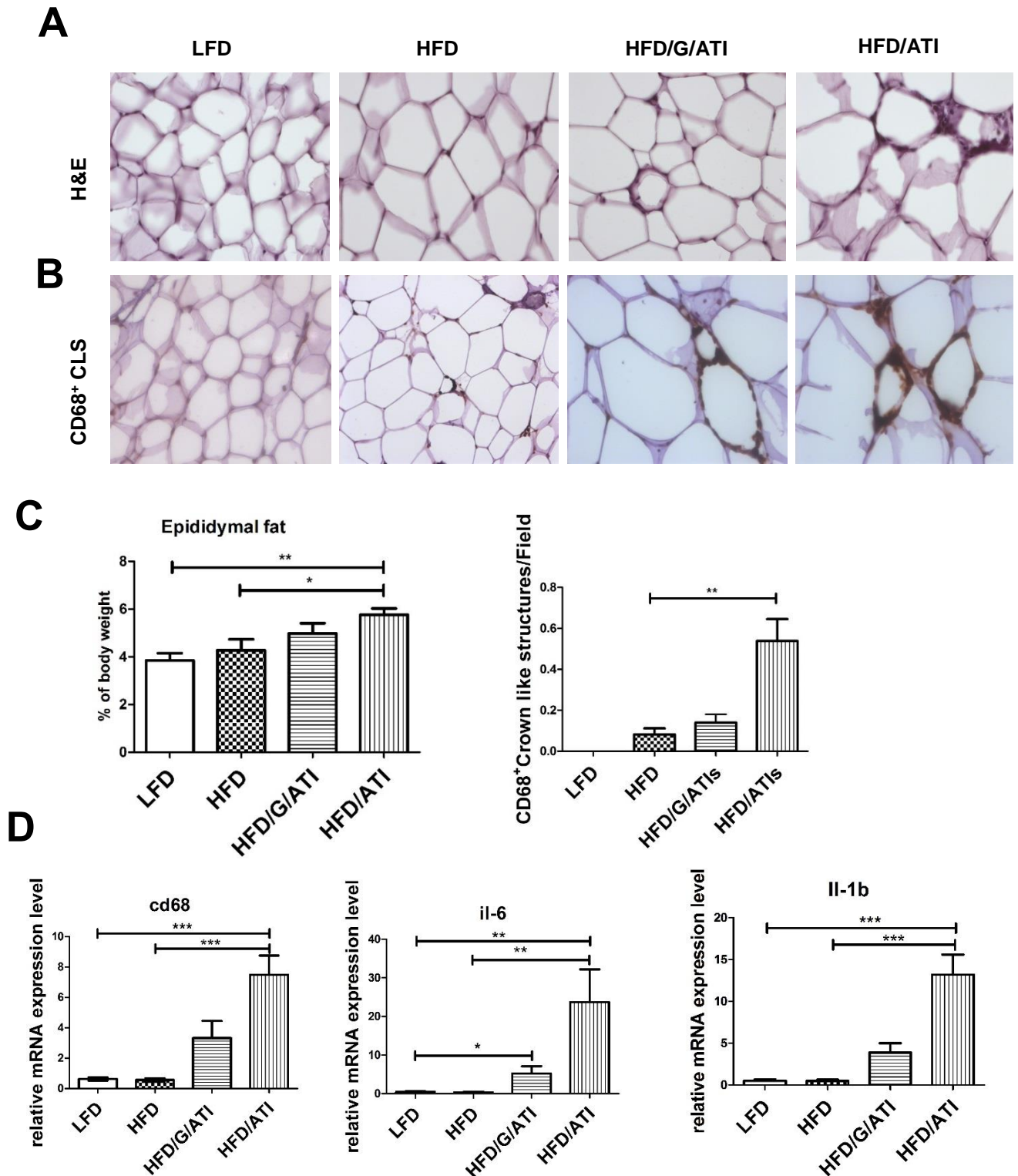
Fig.7 ATI feeding enhances obesity-associated inflammatory parameters. (A) H&E staining (original magnification 40x), (B) Crown like structures (CLS, accumulation of macrophages) in CD68+ stained sections of epididymal adipose tissue in the 4 experimental groups (original magnification 40x). (C) Epididymal fat as % of body weight and the number of CD68+ CLS as determined by morphometry. (D) Transcript levels of cd68, il6 and il1b. Comparisons by ANOVA; data are means ± SEM for 10 representative sections per mouse and 7-10 mice per group; *$p<0.05$, **$p<0.01$, ***$p<0.0$
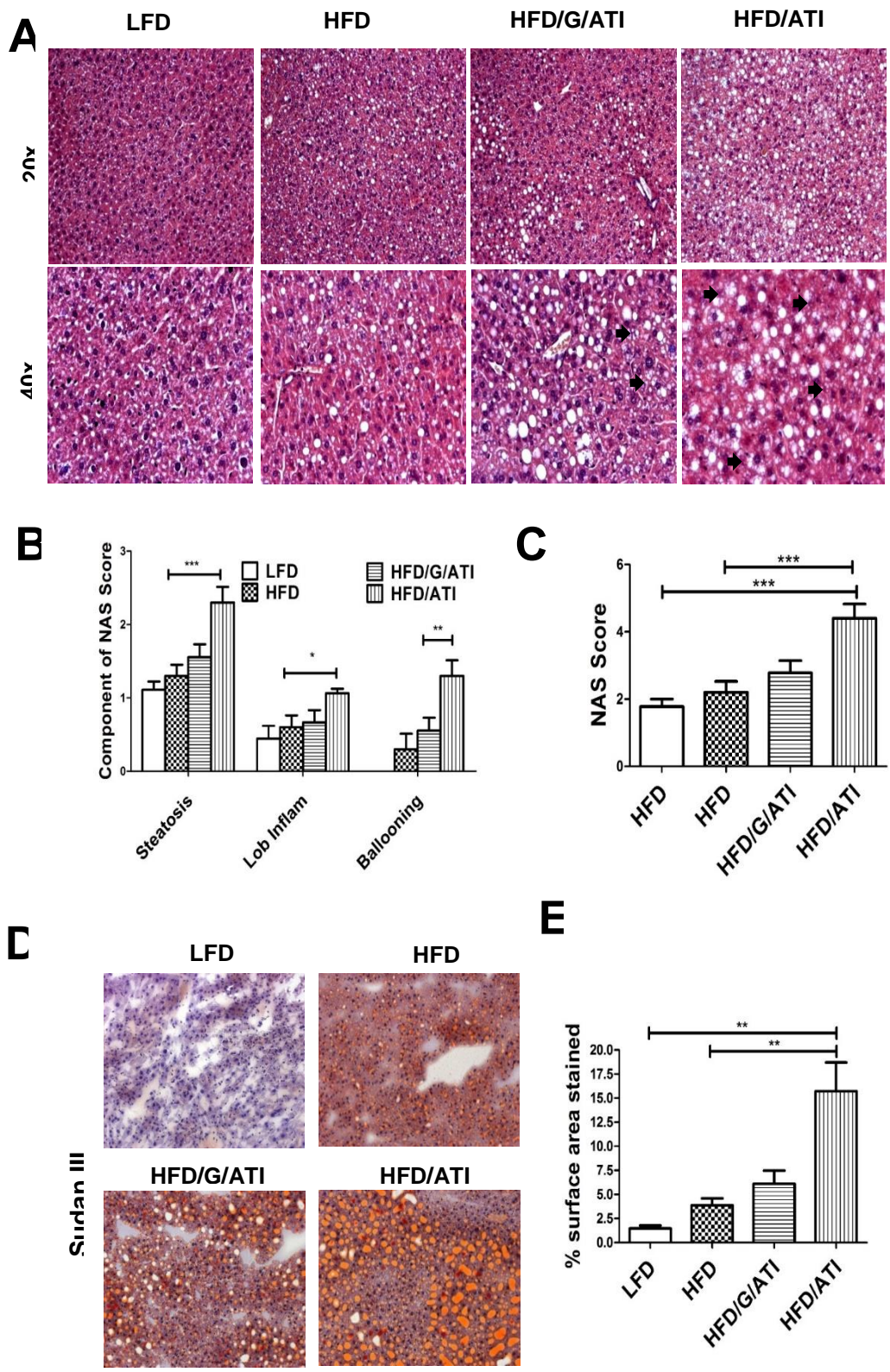
Fig. 8. ATI consumption accelerates liver injury (A) Representative images of H&E stained liver sections (original magnifiction 20x and 40x, upper and lower row, respectively). (B, C) Grading of steatosis, lobular inflammation and hepatocyte ballooning (arrows) according to the NAFLD Activity Score (NAS). (D) Frozen liver sections stained with Sudan III (original magnification 20x). Quantification of % of Sudan III stained area. Comparisons by ANOVA; data are means ± SEM for 5 representative sections per mouse and 7-10 mice per group; *p<0.05, **p<0.01, ***p<0.001.

3.1.5 ATI alone or in a gluten matrix developed hepatic inflammation

Gene expression analysis of the macrophage marker cd68 proinflammatory tumour necrosis factor (tnfa), interleukin 6 (il6) and M2-type (anti-inflammatory) arginase 1 (arg1) and ym-1 (**Fig. 9A-E)** was performed in the mouse livers. cd68 was significantly upregulated in mice on HFD/ATI and HFD/G/ATI vs the HFD alone. In addition, proinflammatory genes il6 and tnfa were significantly upregulated in the HFD/ATI group, with a trend or (lower) significance in the in the HFD/G/ATI group (that received less ATI than the HFD/ATI group) compared to the HFD controls.

Immunohistochemistry on paraffin-embedded livers sections revealed a significantly increased number of CD68$^+$ total macrophages (**Fig. 10A, C)**, and a trend to decreased YM-1$^+$ M2-type macrophages (**Fig. 10B, D)** in HFD/ATI and HFD/G/ATI compared HFD control mice. In addition, FACS analysis showed a significantly higher population of CD11b$^+$F4/80$^+$ (liver resident) macrophages **(Fig. 10F)**. Finally, the CD68$^+$/Ym-1 ratio was significantly higher in the HFD/ATI compared to the HFD alone group **(Fig. 10E)**.
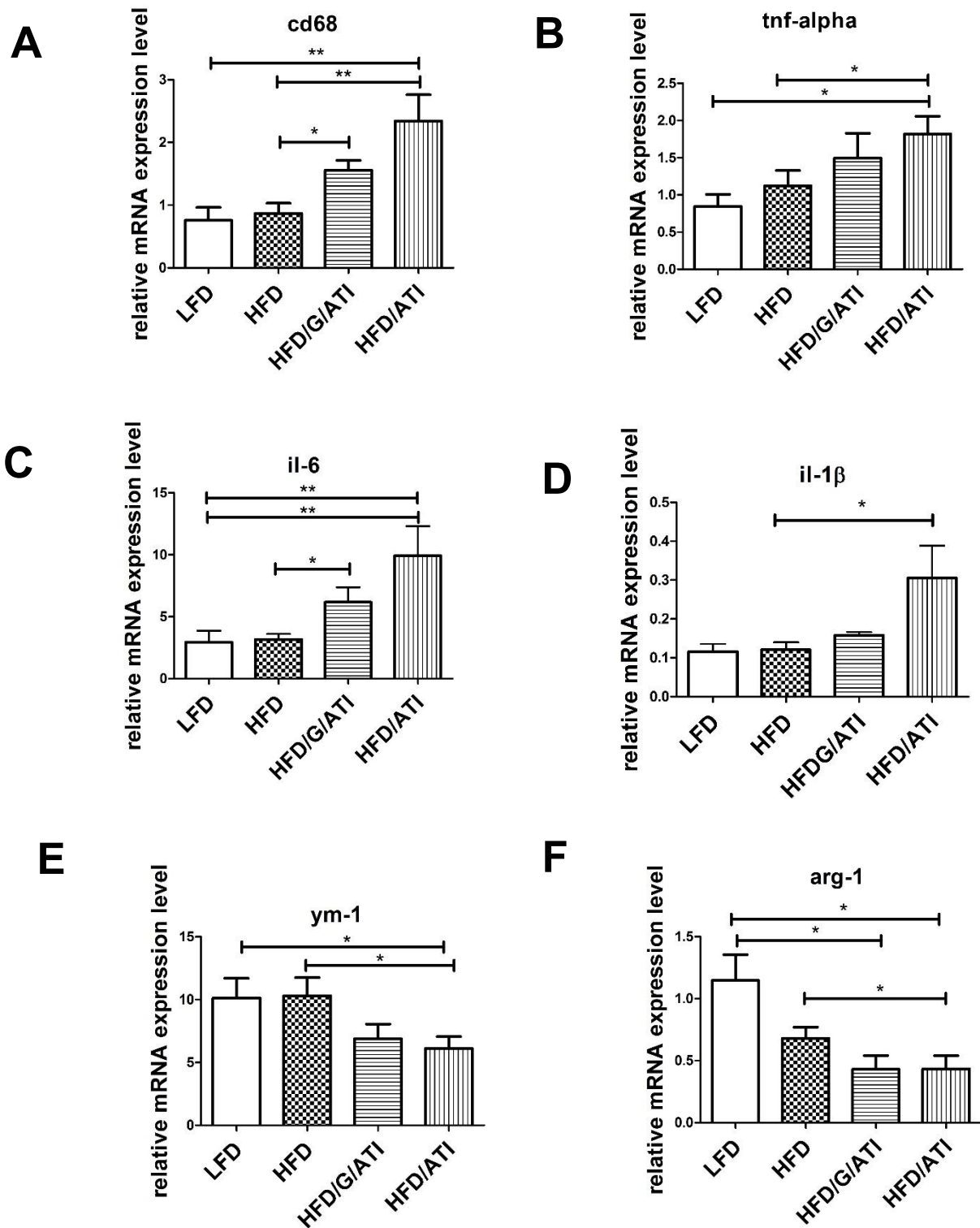
Fig. 9 Gene expression of markers for general, M1- and M2-type macrophages. (A-C) Immunohistochemistry and quantitative morphometry for CD68 and YM-1 positive cells (original magnification 40x). (D) Ratio of total (CD68+) vs M2-type (Ym-1+) macrophages. (E) CD11b+ F4/80+ (liver resident) macrophages (% of CD45 positive total immune cells), as determined by FACS analysis. Comparisons by ANOVA; data are means ± SEM for 10 representative sections per mouse and 7-10 mice per group; *p<0.05, **p<0.01, ***p<0.
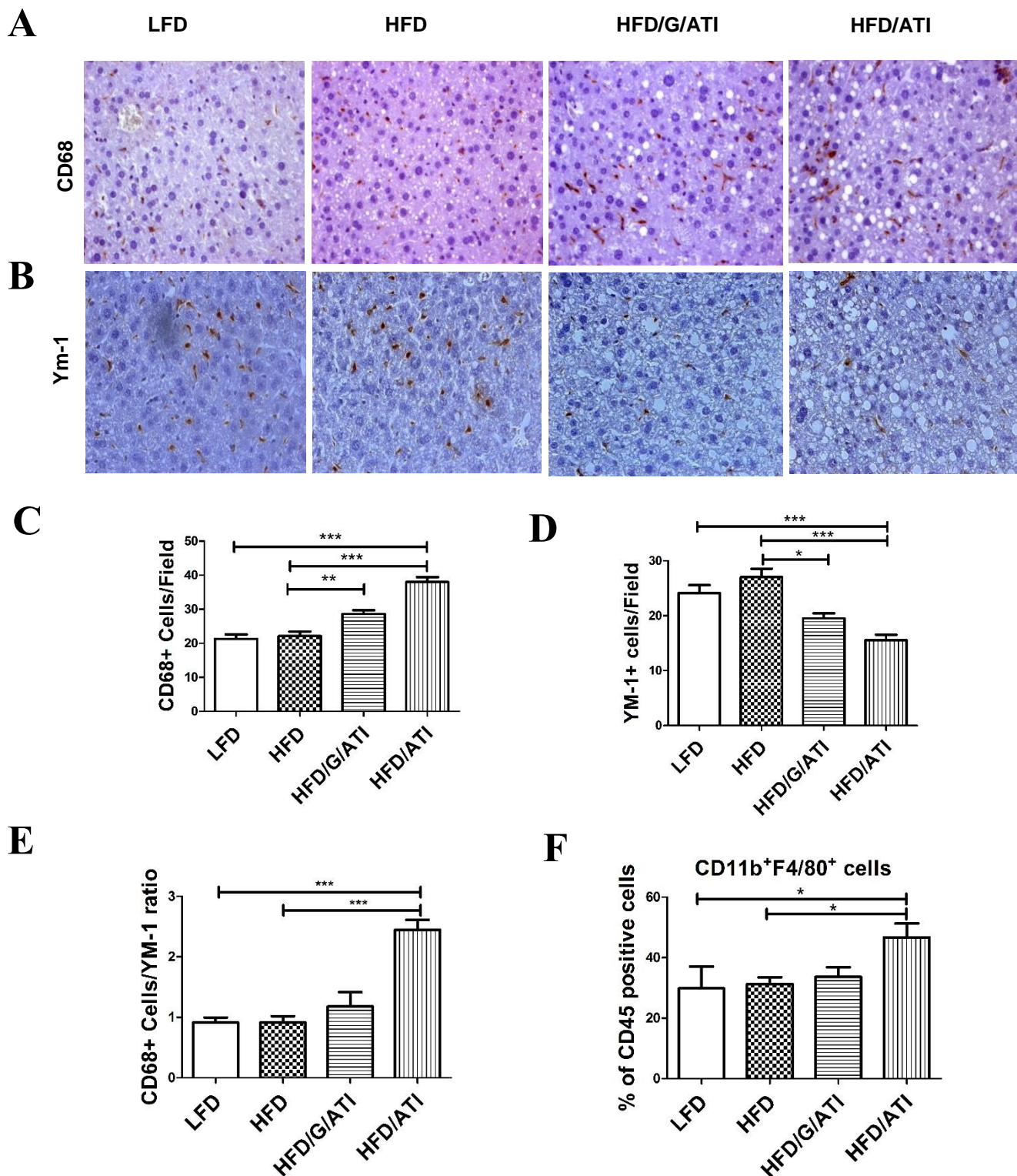
Fig.10 ATI feeding enhances markers of pro-inflammatory NAFLD. (A-F) Hepatic transcript levels of cd68, tnfa, il1b, il6, arg1 and ym1. Comparisons by ANOVA; data are expressed as means ± SEM for 7-10 mice per group; *p<0.05, **p<0.01, ***p<0.001.

3.1.6 Wheat ATI enhance high fat diet-induced liver fibrosis

Fibrosis-related readouts were carried out via gene expression analysis and assessment of liver fibrotic remodelling via Sirius red staining and morphometry. Moreover, staining and morphometry for activated (alpha-Smooth muscle actin positive) myofibroblasts was performed.

Livers of mice fed HFD/ATI and to a lesser extent mice fed HFD/G/ATI showed a significantly accelerated liver compared to the HFD controls, as revealed by gene expression of tgf-beta, mmp9, mmp2, timp1 and col1a1 **(Fig. 11E)**. Sirius red morphometry which better captures parenchymal than the physiological less relevant but abundant portal collagen, increased in the HFD/ATI and HFD/G/ATI fed mice vs mice fed the HFD alone **(Fig. 11A,C)**. This was further confirmed by morphometry for α-SMA, reflecting activation of the fibrogenic effectors cells, demonstrating an enhanced activation of HSC and myofibroblasts in ATI fed vs control mice **(Fig. 11B, D)**. Collectively, all data demonstrate clearly that dietary ATI dose dependently promote HFD induced hepatic fibrosis.
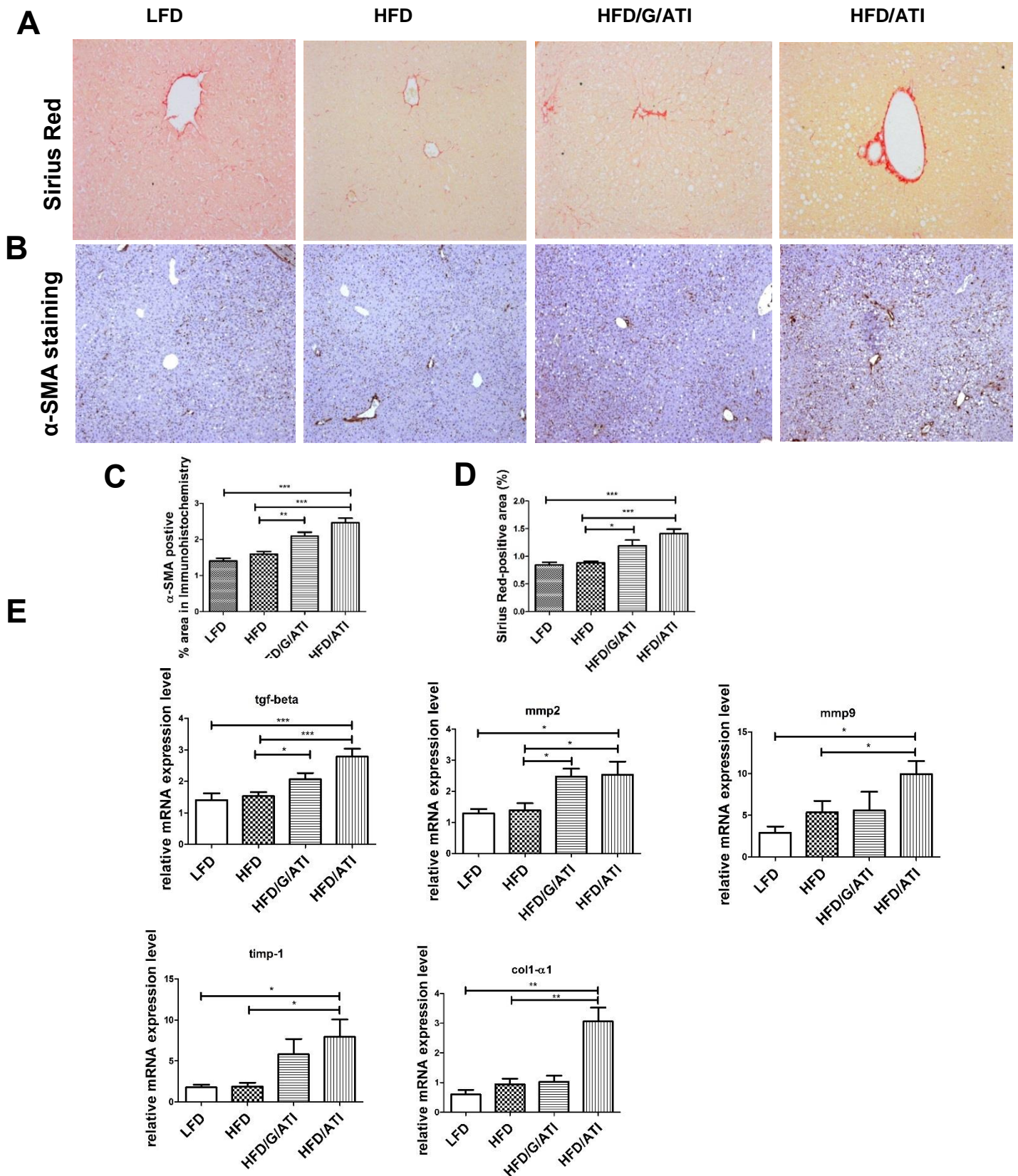
Fig. 11 ATI feeding promotes liver fibrogenesis. (A) Sirius Red and (B) α–SMA immunohistochemistry and (C, D) quantitative morphometry (original magnification 20x). Hepatic transcript levels of tgfbeta, mmp2, mmp9, mmp13, col1a1, timp1 €. Comparisons by ANOVA; data are expressed as means ± SEM of 5 representative sections per mouse and 7-10 mice per group; *p<0.05, **p<0.01, ***p <0.001

3.1.7 ATI feeding increases intestinal macrophage and dendritic cell activation and maturation

As assessed by immunofluorescence and quantitative evaluation, distal small intestinal sections of mice fed the HFD/ATI diet harboured significantly increased CD68+, CD86+, and MHC-II+ dendritic cells/macrophages (**Fig.12A,D**) compared to mice fed the HFD alone. Moreover, intestinal transcript levels of il1b, tnfa and il6 were significantly increased in the HFD/ATI vs the HFD group (**Fig.12D**).
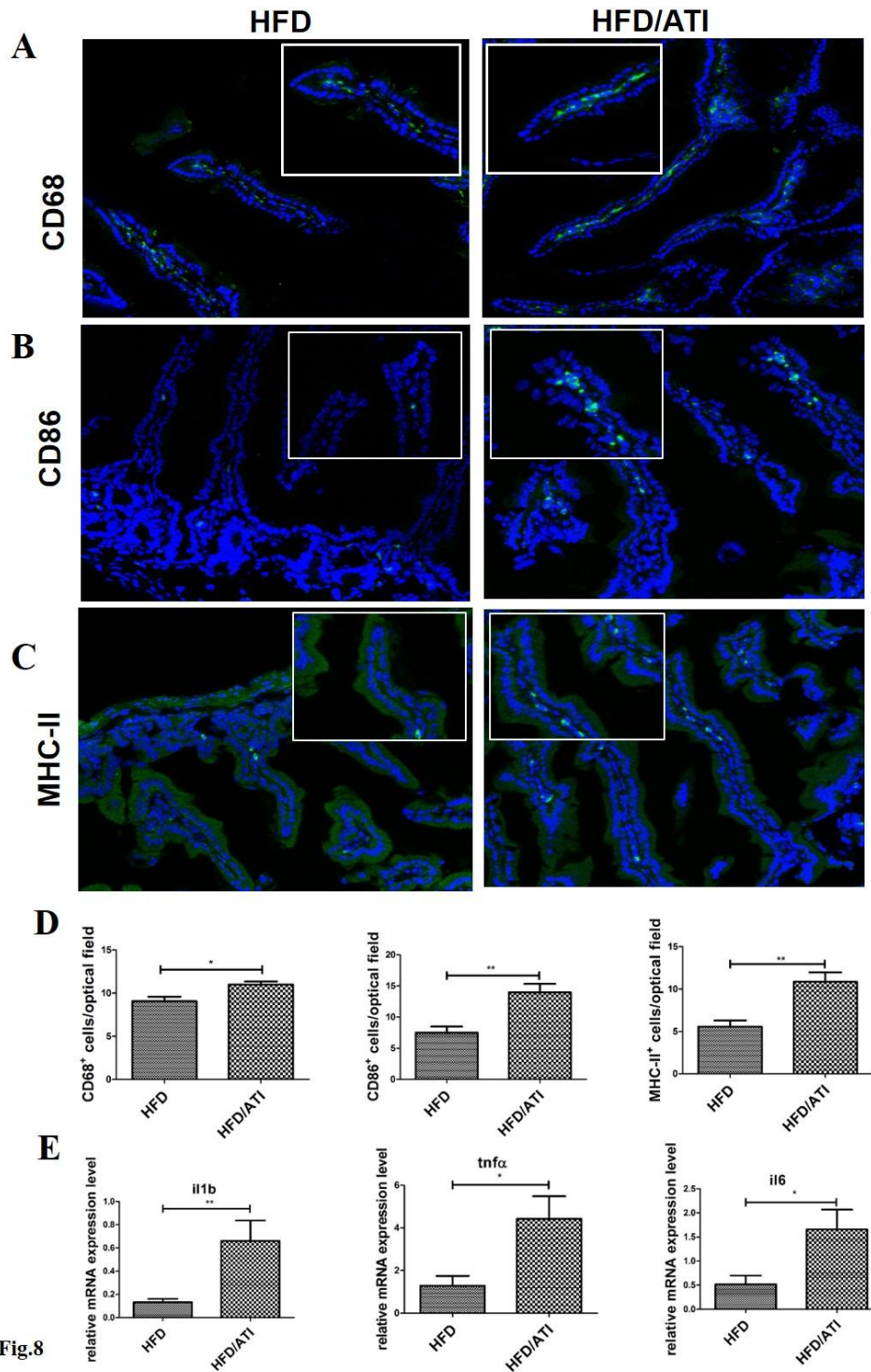
Fig.12 ATI feeding increases intestinal macrophage and dendritic cell numbers, activation and maturation. (A-C) CD68, CD86 and MCH-II expressing cells in the terminal ileum; scale bar: 100 and 50μm. (D) Morphometric quantification of CD68, CD86 and MHC-II positive cells. (E) Transcript levels of il1b, tnfα and il6. Comparisons by ANOVA; data are expressed as means ± SEM of 6 mice per group and 5 representative sections per mouse; *$p<0.05$, **$p<0.01$, ***$p<0.001$.

3.2 Dietary wheat amylase trypsin inhibitors promote liver fibrosis in murine model of biliary fibrosis

3.2.1 ATI feeding causes hepatomegaly and increased serum liver enzymes

Mdr2-/- FVB mice that spontaneously develop severe biliary fibrosis at age 6-12 week[43] were fed the ATI containing diet as above from week 6 till week 12 of age with 0.7% of the noninflammatory corn protein zein as ATI but with a normal fat content (see Methods section No. 2.1.7). ATI-fed Mdr2-/- FVB mice showed a significant increase in liver weight (but no increase of body weight) compared to the ATI-free control group (**Fig.13A**). Moreover, these mice displayed significantly increased serum ALT, AST levels vs the control group indicating more severe inflammation and cholestasis (**Fig.13B-D**).
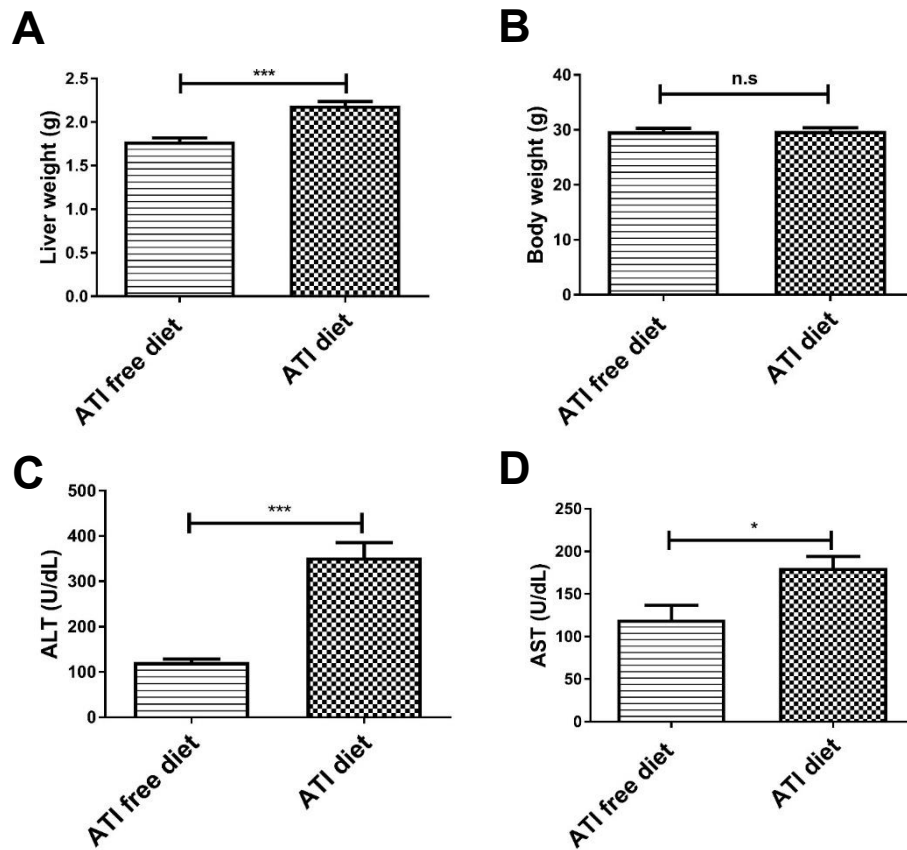
Fig.13 ATI feeding increases liver weight and serum inflammatory and cholestatic enzymes in biliary fibrotic Mdr2-/- FVB mice. (A) Gain in liver weight in ATI fed group compare control (B-D) Serum ALT, AST levels are significantly increased in ATI fed mice compare to control group. Data are expressed as means ± SEM of 5 mice per group and 5 representative sections per mouse; *p<0.05, **p<0.01, ***p<0.001.

3.2.2 Nutritional wheat ATI increase the expression of hepatic genes related to inflammation and fibrogenesis.

Transcript levels of Il1b and tnfa were highly upregulated in the ATI fed Mdr2-/- FVB mice compared to control mice fed the ATI-free diet **(Fig.14A, B)**. Expression of fibrosis-related genes (acta=asma, col1a1, col3a1, mmp13, timp1, mmp9) were significantly increased in ATI fed group compare to control group **(Fig. 14C-H)**.
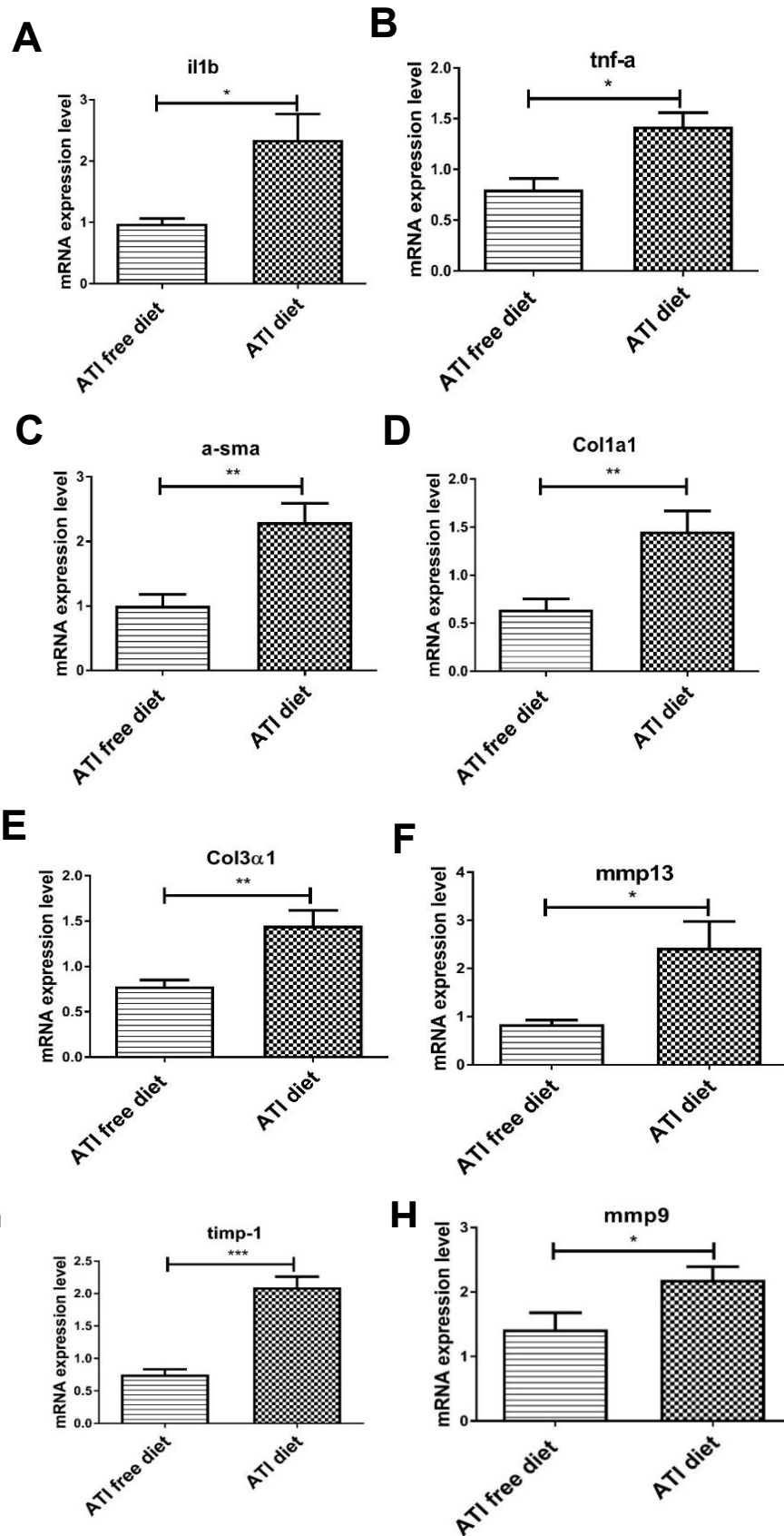
Fig.14 Hepatic expression of inflammation and fibrosis related genes. (A, B) Transcript levels of il1b, tnfa; (C, D, E) Fibrosis related transcripts asma, col1a1, col3a1; (F, G, H) transcript levels of mmp9, mmp13 and timp19. Data are expressed as means ± SEM of 5 mice per group and 5 representative sections per mouse; *p<0.05, **p<0.01, ***p<0.001.

3.2.3 ATI feeding increases ductular reactions and hepatic macrophage infiltration

H&E staining revealed expansion of ductular proliferations in ATI fed compare to the ATI free group **(Fig.15 A)**. In addition, CD68 immunohistochemistry demonstrated an increased infiltration of CD68$^+$ macrophages in ATI fed mice **(Fig.15 B, C)**.
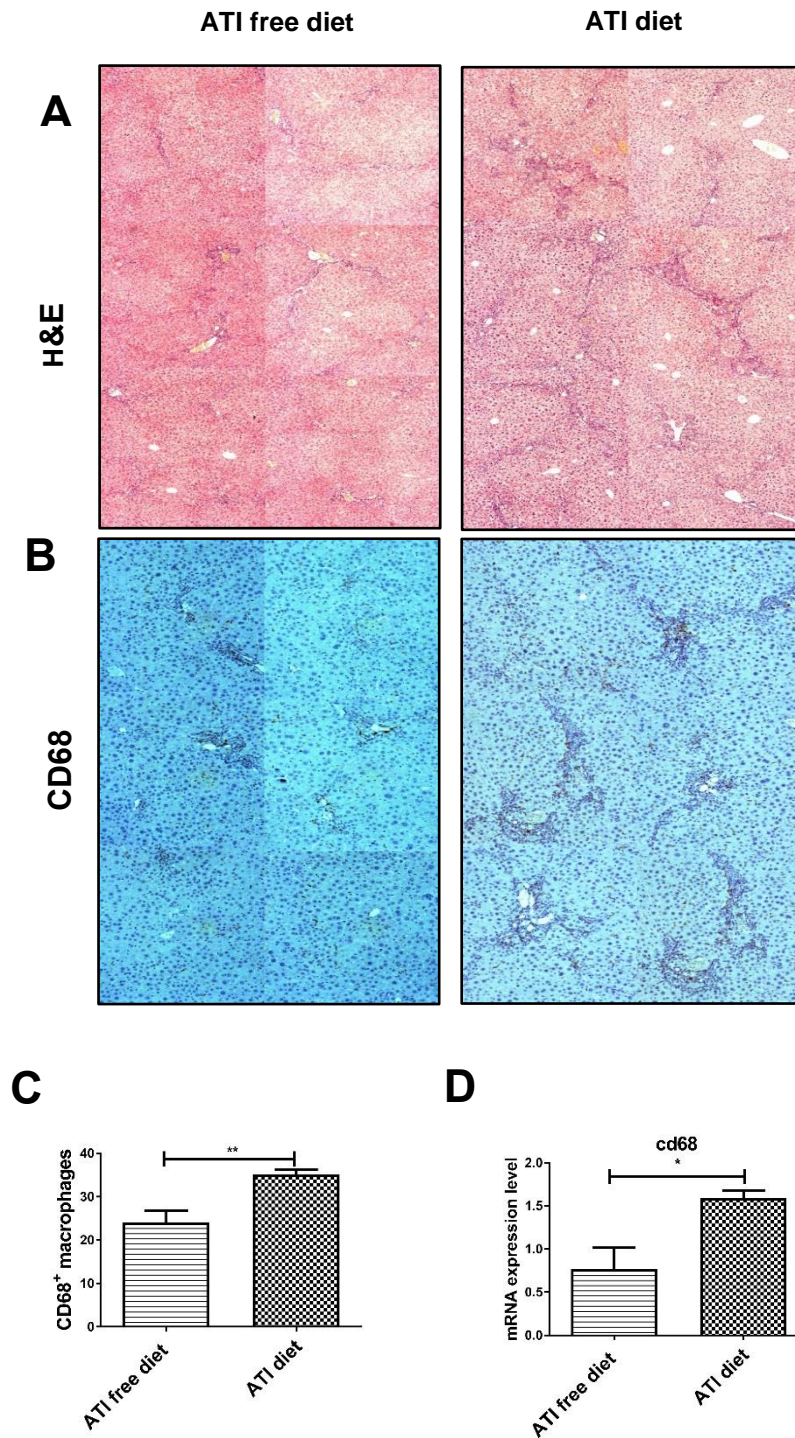
Fig.15 ATI feeding worsens ductular proliferation and inflammatory responses. (A) Representative low magnification (10x) images of H&E stained section of ATI fed mice compared to ATI-free controls. (B, C) CD68 immunohistochemistry and quantification of ATI fed vs ATI-free controls. (D) Hepatic transcripts levels of cd68, data are expressed as means ± SEM of 5 mice per group and 5 representative sections per mouse; *p<0.05, **p<0.01, ***p<0.001.

3.2.4 ATI worsen fibrosis in Mdr2-/- FVB mice

Collagen (Sirius Red) (**Fig.16 A, C)** and alpha-SMA immunohistochemistry **(Fig.16 B,D)** showed a significantly increased accumulation of collagen and number of activated HSC and myofiboblasts in livers of ATI-fed vs ATI-free mice.
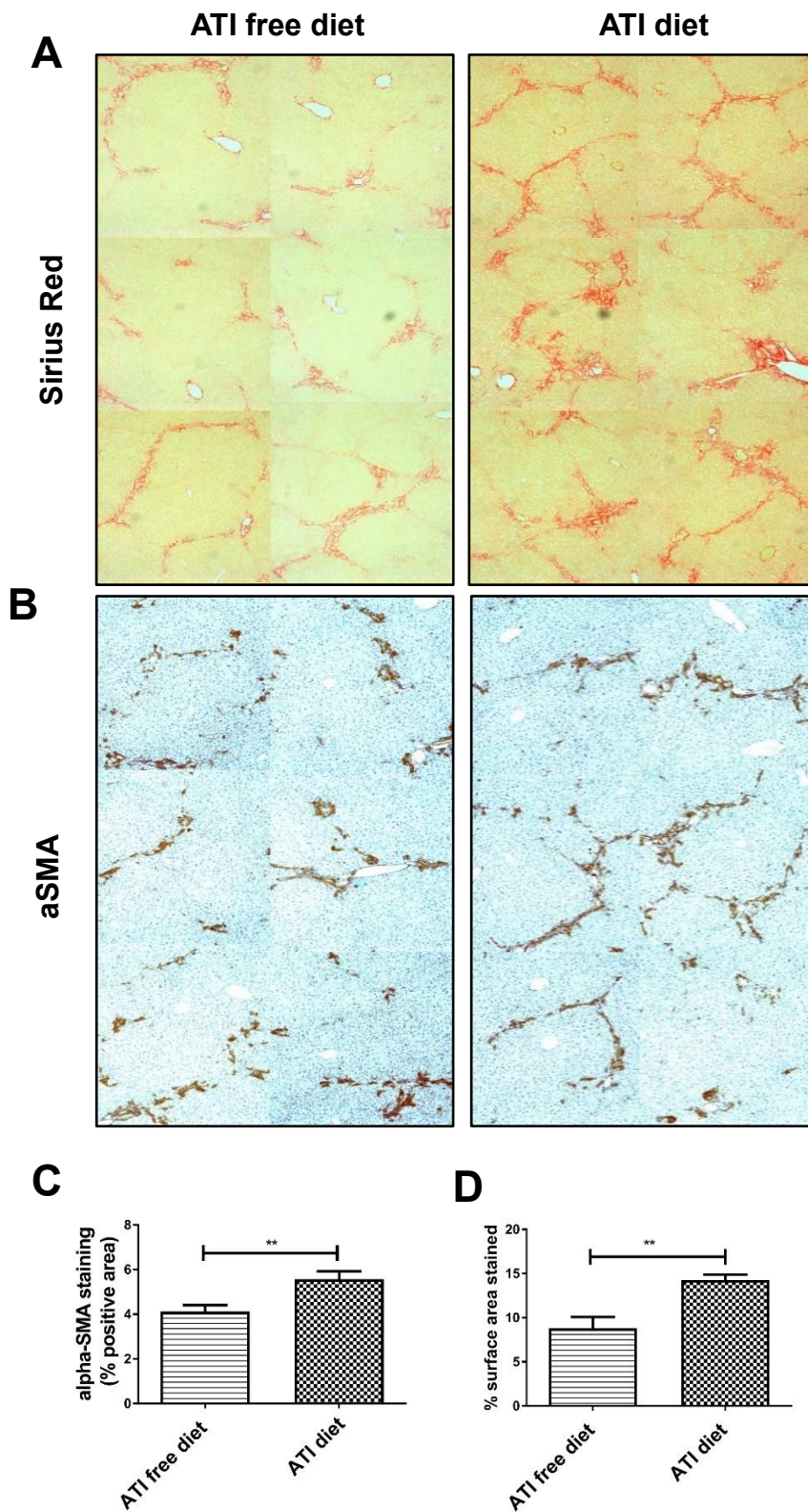
Fig.16 ATI feeding accelerates liver fibrosis progression in Mdr2-/- FVB mice. (A, C) Representative low magnification images (10x) and morphometrical quantification of collagen (Sirius Red stain). **(B, D)** α-SMA–positive activated HSC/my fibroblasts and morphometrical quantification. Data are expressed as means ± SEM of 5 mice per group and 5 representative sections per mouse; *p<0.05, **p<0.01, ***p<0.001.

4. Discussion

One of the major component of human diet is wheat that been introduced roughly 12,000 years ago,[77] and different wheat varieties have been commonly used in the production of numerous foods. While wheat has become the major staple on a global scale, wheat related inflammatory diseases, such as wheat allergies and celiac disease have increased in prevalence.[78]

Innate immune cells (macrophages, monocytes, DCs and polymorphonuclear leukocytes) sense various microbial and chemical stimuli by several surface receptors such as toll like receptors. These stimuli modulate and prime adaptive immune cells priming[79] in the intestine and other organs, including the liver.

The intestinal microbiota possess approximately 100-fold more genetic information that the mammalian body and much of this information is conveyed to the host via secretion of various metabolites and hormones directly into the gut and the intestinal lamina propria. Additionally, the liver is a central organ located between the intestine and other organs representing a unique "buffer zone" that directly receives signals from the gut that stem from, e.g. nutrients, metabolites toxins, or hormones. Therefore, the interaction between the intestine and the liver including also the immune systems of these organs and the first hepatic metabolism of gut derived nutrients, toxins and metabolites in the liver has gained great attention. In this context and expanding number of studies both in vivo and in vitro have focused on this gut-liver axis demonstrating its relevance in health or disease of both organs and other organs of the body. Primary diseases that are affected by the gut-liver axis are, e.g. alcoholic (ALD) and non-alcoholic fatty liver disease (NAFLD), non-alcoholic steatohepatitis (NASH), cholestatic liver diseases, hepatocellular carcinoma (HCC) and liver fibrosis/cirrhosis and their further complications in general.[54] Importantly, the composition of the diet, including its direct metabolic effects and its secondary effect on the composition of the intestinal microbiota has the potential to significantly modify the course and severity of NAFLD in this triangular of dynamic interaction the gut, diet and the liver.[80]

The liver that is directly connected to the vascular outflow of the intestine via the portal vein acts also a first line of defence against gut-derived invaders and other agents[55]. Here, wheat ATI are newly discovered triggers of innate immunity in intestinal myeloid cells via the TLR4-MD2-CD14 complex.[17] Since, the activation

signals triggered by ATI in the intestine are propagated from the gut to the periphery, possibly by migration of the activated myeloid cells to the mesenteric lymph nodes and beyond, [17, 81, 82] we speculated that nutritional ATI might especially affect the gut liver axis and thus potentially exacerbate chronic liver disease, especially the metabolic liver disease of NAFLD/NASH. Indeed, in this thesis further evidence of the inflammatory role of nutritional ATI was provided by demonstrating that they worsened chronic liver disease in preclinical models of NASH and biliary fibrosis in representative mouse models of these liver diseases. Based on these studies, it is likely that similar effects will also see in patients with these chronic liver diseases.

4.1 Wheat ATI promote obesity, adipose tissue inflammation and insulin resistance

Around 1.9 billion people worldwide are obese, i.e., have a body mass index above 30, with an increased risk for various health related problems such as atherosclerosis, stroke, myocardial infarction, T2D, NAFLD/NASH, and with an increased risk to develop certain common cancers[83]. Taken together, obesity has been associated with more than 65 comorbidities contributing to a high overall and escalating mortality.[84] Moreover, the obesity associated metabolic syndrome (MetS), including dyslipidemia, IR/T2D and hypertension are tightly linked to NAFLD progression[85], although these entities can also exist independently and do not show a complete overlap, indicating that still ill-defined independent pathogenic factors are in involved in NAFLD/NASH pathogenesis.[86]

In this context, NAFLD progression towards NASH is favoured upon the development of obesity and IR at the level of both adipose tissue and the liver [87], and since NAFLD is one newly discovered hepatic manifestation of the MetS.[88] In accord with this concept, the HFD/ATI and ATI/G/ATI diets did not only promoted obesity, but also dyslipidemia, IR and finally liver inflammation and fibrosis, with an escalating trend in mice fed the HFD/G/ATI vs the HFD/ATI diet (the latter containing more ATI than the former). Furthermore, the visceral fat compartments (epididymal, mesenteric, and inguinal) were significantly expanded in mice on the HFD/ATI and HFD/G/ATI as compared to the HFD controls, despite no change in energy consumption. The underlying mechanism of ATI mediated weight gain could be explained (although yet to be substantiated) via several pathways e.g. ATI may trigger a shift in microbiota since reduction of 20% fecal *Bacteroidetes* has been

associated with 150kcal more energy extraction from food per day in lean individuals.[89] Moreover, intestinal permeability especially in the frame of gut liver axis could also be one of the mechanism in physiology and pathophysiology of ATI mediated weight gain and the resultant non-alcoholic fatty liver disease phenotype.[90] Alternatively, ATI may mimick dietary fat induced LPS internalization and thus draining of LPS to mesenteric lymph nodes and release of TNF-alpha.[91]

There was also a moderate correlation between the mesenteric and epididymal fat expansion seen in these mice.

Inflammatory processes in obesity and the MetS are prominently found in the expanding visceral, but recently also white adipose tissue[92], with an increase of mainly macrophages and a shift of their anti-inflammatory towards a proinflammatory phenotype.[83] In these adipose tissues, macrophages changes both regarding phenotype towards proinflammatory M1-polarized macrophages and towards increased numbers, secreting proinflammatory cytokines, e.g., CCL2 (MCP-1), TNF-α and IL-6, in contrast to the usual M2-type macrophages that express anti-inflammatory Arg-1, IL-10, and surface markers YM-1 and CD206. This switch towards increased ratio of M1-polarized proinflammatory phenotype over M2-type macrophages is the major feature of inflammation of adipose tissue in obesity and the liver in NASH, has been linked to IR and other metabolic complications, e.g., vascular inflammation.[93] The central importance of innate immunity and the relevance of the further downstream adaptive immunity in obesity and the associated MetS, where gut and liver inflammation are involved have been highlighted in recent reviews.[54, 59, 94]

That the severity of NAFLD is tightly linked to adipose tissue inflammation was also demonstrated by the characteristic, increased macrophage infiltration with formation of crown-like structures (CLS), a source of pronounced expression of pro-inflammatory genes.[95] In the present thesis, a marked upregulation of inflammatory genes in the epididymal fat compartment of HFD/ATI fed compared to the HFD fed control was observed, followed by an intermediate upregulation in the HFD/G/ATI, again correlating with the dose of ATI consumed that was approximately 50% of the HFD/ATI group. Moreover, the HFD/ATI fed mice had bigger adipocytes and thus increased fat stores, in line with the adipose tissue expansion measured as weight increase, compared to the controls. Taken together, the significant expression of inflammatory genes with pronounced formation of crown like structures in the

epidydimal fat tissues demonstrates that ATI feeding in mice promoted not only body weight gain but also also triggered inflammation in the visceral adipose tissue.

CLS are mostly composed of macrophages and are considered hubs of adipose tissue inflammation, with increased cytokine expression and secretion, mainly in visceral and epididymal fat depots.[96,76,97] High fat diet feeding increases the expression of M1 macrophage markers (e.g., iNOS, TNF-alpha) and decreases the expression of M2 macrophage markers (e.g., IL-10, Arg-1).[93] These adipose tissue macrophages communicate with the liver and other organs via their cytokine and adipokine secretion[98]. Vice versa, liver derived mediators may signal to the adipose tissue[99]. It is still unclear how far adipose tissue and liver macrophages may receive signals from the gut, or even may be replenished by activated monocytes-macrophages from the intestine.

ATI feeding has been shown by us to lead to emigration of ATI-activated monocytes-macrophages (or migratory dendritic cells) from the gut to the surrounding mesenteric lymph nodes and likely further to the periphery[53]. From the data presented in this thesis, it is thus likely that the increased CLS structures and inflammation in epididymal fat tissues and the M1-type macrophage accumulation in the inflamed liver (HFD/ATI>HFD controls) derive from enhanced monocytes-macrophage-DC activation and that these cells migrate out of the intestine to these target organs. Notably, adipose tissue and the liver are those organs where the HFD and obesity related pathology is already ongoing, confirming further the gut-liver axis paradigm. However, additional studies are needed and on the way, to track ATI-activated myeloid cells from the gut to the affected organ(s).

4.2 Chronic feeding of ATI feeding worsen histological features associated with nonalcoholic fatty liver disease

Steatosis, hepatocyte ballooning, and intra-acinar and portal inflammation are the histological hallmarks of NASH. NASH related fibrosis starts from zone 3 and perisinusoidally, with portal/periportal fibrosis developing from stage 2 on and progressive architectural remodelling finally leading to cirrhosis.[28] NAFLD/NASH progression was staged (fibrosis) and graded (inflammation) via the NAS score that was adopted for mice, in alignment with studies.[25] Histologically, higher individual and sum scores for steatosis and lobular inflammation, including hepatocyte ballooning, were observed in the HFD/ATI fed mice compared to the isocalorically

fed ATI-free controls. In the same line, accumulation of lipid droplets in the hepatocytes that was semi quantified via Sudan III stained frozen liver sections revealed a significant more pronounced hepatic lipid accumulation in the HFD/ATI group. Therefore, hepatic lipid accumulation went hand in hand with visceral and peripheral adipose tissue expansion and inflammation, in support of the close communication between these organs, and in line with the adverse effect of nutritional ATI on metabolism, obesity, IR and NAFLD progression. Currently, it is unclear if the liver is the prime target organ of the intestinal ATI-effects that would be followed by adipose tissue inflammation, or if both organs are targeted independently, e.g. by monocyte-DC emigrating from the gut to both these tissues.

4.3 Chronic feeding of ATI promotes multiple features of NAFLD associated hepatic inflammation

Inflammatory cytokines and chemokines, e.g. IL-6, TNF-α, IL-1β and CCL2, promote steatosis and fibrosis during NASH progression. These mediators are secreted by resident liver cells but especially upon infiltration of circulating immune cells into the liver.[100] These inflammatory mediators are mainly secreted by macrophages that therefore play a key role for the progression of fibrosis and up to the development of hepatocellular carcinoma.[101-103] These cytokines are secreted by activated macrophages mainly in response to stimulation of the innate immune receptors (TLR4) by free fatty acids and cholesterol, or by endocytosis of or mediators released by nectrotic/apoptic hepatocytes.[104, 105] Moreover, the enhanced pro-oxidative environment in NASH promotes their activation by ROS or oxidized lipid products (ref). Apart from inflammation in the liver or adipose tissue, circulating endotoxin levels appear to be increased in advanced NASH and fibrosis due to loss in the integrity of the intestinal barrier.[106-108] In murine models of NASH and in NASH patients, the liver resident macrophages and blood monocytes are also more sensitive to lower levels of endotoxins.[109, 110] These studies emphasize the importance of the gut-liver axis in in the pathogenesis and progression of NAFLD.[111]

NAFLD is a spectrum of liver diseases that include simple steatosis, fatty liver plus inflammation and hepatocellular ballooning degeneration (NASH), often progressing to advanced fibrosis in the absence of significant alcohol consumption.[112] Therefore, worsening of all these aspects of murine NAFLD/NASH after only 8 weeks of ingestion of ATI at a daily dose comparable to human average consumption and in

the absence of enhanced calorie intake, is remarkable. All results, obtained with a wide spectrum of molecular, metabolic, physiological, and inflammation as well as fibrosis related readouts clearly demonstrate a worsening of HFD induced NAFLD, which represents a very mild model of human NAFLD that usually does not show significant liver and adipose tissue inflammation or fibrosis. Here, ATI consumption moved all the latter parameters into the significantly elevated and pathological range, indicating that nutritional ATI are a relevant second hit to NASH development, likely with similar relevance in humans, a hypothesis that is currently tested in a clinical study performed at TIM and the Dept. of Medicine 1 of UMC Mainz. ATI/HFD fed mice demonstrated significantly elevated levels of cd68, il6, and tnfa transcript, whereas the anti-inflammatory M2-type macrophage/DC markers arg1 and ym1 were suppressed. In this line, the modulation of hepatic inflammation by nutritional ATI was further confirmed by elevated numbers of CD68+ macrophages in the ATI while the number of YM-1 positive M2-type macrophages was reduced. Moreover, FACS analysis revealed a significantly increased number of CD11b$^+$F4/80$^+$ (resident) liver macrophages in the HFD/ATI vs HFD alone fed mice, with an increased trend in the HFD/G/ATI group (that received about half the ATI dose of the HFD/ATI group) vs the HFD fed controls.

4.4 Chronic feeding of ATI feeding enhances murine NAFLD related hepatic fibrosis

Since NAFLD/NASH is a progressive disease, with advanced fibrosis/cirrhosis being the most relevant clinical endpoint in current therapeutic studies reported by us[1], several fibrosis related parameters were assessed via gene expression measurements and quantitative morphometry of liver sections through Sirius red and alpha smooth muscle actin morphometry. Here, most parameters were (highly) significantly increased in the HFD/ATI fed group vs the HFD controls. There was a clear trend of increased hepatic collagen deposition, as measured biochemically via HYP content, in HFD/ATI vs the control group, a parameter that gives too much weight to the physiologically less relevant portal tract collagen vs the more relevant perisinusoidal collagen which is better captured by SR morphometry that demonstrated significant differences. However, the study period was very short, 8 weeks of feeding, and a feeding for 12-24 weeks would for sure have yielded significant Hyp results. This was by intention, to test how far the readouts would

allow a short-term study that in this case already yielded clear results (except for the trend in Hyp), a scenario that is far more attractive than a lengthy animal study.

In summary, the presented study implicates dietary ATI from wheat as potent pro-inflammatory and pro-fibrotic nutritional drivers of NAFLD/NASH. This effect occurs at a daily intake that is comparable to average human consumption of wheat products. Based on these results, a clinical trial is on its way.

4.5 Chronic feeding of ATI accelerates liver fibrosis in murine model of biliary fibrosis

TLR4 has been implicated as a promoter of liver fibrosis in general.[50][51] Moreover, research is undergoing to mechanistically identify players in the progression of biliary fibrosis diseases that lack efficient treatment[113]. Recently, a report implicated TLR4 signaling in pathogen-associated biliary fibrosis (PABF).[52] Notably, nutritional activators of TLR4 in liver fibrosis in general and in biliary fibrosis in particular had not been identified nor studied. Here, the additive role of ATI as nutritional activator of TLR4 signalling to further worsen liver fibrosis in a recognized mouse model of PSC is relevant. In the present work, ATI feeding for only 6 weeks has significantly increased liver weight, serum ALT, AST reflecting enhanced liver injury and fibrosis compared to the control diet fed Mdr2-/- FVB mice. Moreover, inflammatory makers (cd68, il1b, tnfa) were highly expressed in ATI fed Mdr2-/- FVB mice vs the ATI-free controls. In line with this, ATI fed Mdr2-/- FVB mice showed significantly increased numbers of hepatic CD68+ macrophages compared to the controls. Likewise, enhanced ductular reactions extending towards the parenchyma upon ATI feeding were found. Importantly, these ductular reaction are central drivers of liver fibrosis in biliary and advanced non-biliary liver diseases.[1, 43, 114] As a results, an increased deposition of SR-stained collagen and number of alpha-SMA+ myofibroblasts were observed in ATI fed mice compare to control mouse. Based on these and prior preclinical data, the Tim and Hamburg University Medical Center currently perform a clinical study in patients with PSC on a largely ATI (wheat)-free vs a normal ATI (wheat)-containing diet.

4.5 Conclusion

The worldwide rising incidence and prevalence of NALFD and its severe variant NASH and liver fibrosis require efficient preventive and therapeutic intervention. Therefore, in addition to life style changes and a search for therapeutic targets and

novel drugs for the treatment of NAFLD/NASH patients and patients with advanced liver fibrosis, dietary factors that are ubiquitous may be relevant. Lack of caloric value but are inflammatory in nature triggering a cascade of nacre-inflammation in NAFLD/NASH patients via a recently known paradigm "gut liver axis" require special attention. In this context, I studied the effect of nutritional wheat amylase trypsin inhibitors that activate intestinal myeloid innate immune cells via stimulation of the TLR4-MD2-CD14 receptor complex in the pathogenesis of NAFLD/NASH in a murine model of non-alcoholic fatty liver disease, as well as in a model of secondary biliary fibrosis. After only 8 weeks of ATI consumption within a HFD chow, there was a significant increase in (visceral) adipose tissue expansion with enhance inflammatory cells, mainly M1-type macrophages. These mice fed also showed a significantly more severe liver phenotype, including, steatosis, inflammation, apoptosis, and fibrosis, and were also more glucose intolerant compared to mice fed the isocaloric HFD alone. Additionally, upon 6 weeks of ATI feeding, secondary biliary fibrotic Mdr2-/- FVB mice showed increased ductular reactions and liver fibrosis compared to Mdr2-/- FVB mice fed the ATI-free, isocaloric control diet. Taken together, ATI feeding acted as a highly relevant second hit and worsen chronic liver disease in preclinical models of NASH and secondary biliary liver fibrosis in mice. These results do already serve as a basis for nutritional clinical studies in patients with NAFLD/NASH and PSC who are consuming a largely ATI (wheat)-free vs an normal, ATI (wheat)-containing diet.

5. Add-on of recent experiments on mechanisms of macrophage polarization in experimental NASH

Deletion of IL-4 receptor Alpha on macrophages in murine nonalcoholic steatohepatitis (NASH)

5.1. Introduction

Liver macrophages are a mixed population and are either resident phagocytes (Kupffer cells) or derive from the circulating monocytes (monocyte-derived macrophages).[115] In patients with chronic liver disease, the chemokines CCL2, CCL3 and CCL6 attract blood monocytes to the injured liver that serve as precursors of liver macrophages and dendritic cells.[116-118] With acute or protracted liver injury, huge number of monocytes infiltrate the injured liver occurs and may represent the major macrophage pool. In line with this prominent infiltration and the large number of resident Kupffer cells, macrophages are central regulators of liver immune homeostasis and fibrosis (Kazankov K et al, Nat Rev Gastroenterol and Hepatol, in press). Moreover, liver macrophages critically modulate either fibrosis progression or regression, depending on the disease stage and context, especially in NASFLD/NASH.[119] It has been reported that a dysregulated and protracted repair processes, as in chronic inflammation, M2-type macrophages that are activated via IL-4 and IL-13 in type 2 immunity promote progression of pathological fibrosis in different organs including the liver.[120] Moreover, the serum levels of IL-4 and IL-13 were increased with the severity of liver fibrosis (F3-F4>F0-F1) in patients with non-alcoholic steatohepatitis.[121] Both IL-4 and IL-13 that are mainly produced by Th2 T cells propagate their intracellular signal via two different but overlapping receptors having a common subunit of the interleukin-4 receptor, the IL-4Rα chain, [122-125] and both cytokines (IL-4 and IL-13) activate the IL-4Rα together with the interleukin-4 type II receptor expressed on resident and infiltrating myeloid cells.[126] Our group has previously shown that the genetic deletion of the IL-4Rα in general and similarly on macrophages retarded fibrosis progression in carbon tetrachloride induced liver fibrosis.[127] Therefore, the aim of this study was to study the role IL-4Rα, and therefore of IL-4/IL-13 signalling in a representative mouse model of NASH, using IL-4Rα deleted mice.

5.2. Methods

8-week-old male Balb/C wild type mice and Balb/C mice with a general or macrophage specific deletion of IL4Ra (Balb/C IL4R$^{-/-}$ and LysM^{cre}IL4Rα$^{-/lox}$) mice were fed a choline-deficient, L-amino acid-defined (CDAA) for an additional 12 weeks. During feeding, evolution of body and liver/spleen weights was monitored, and intraperitoneal glucose tolerance were carried out before the day of sacrifice. Inflammation and fibrosis related parameters were determined as outlined in the previous chapters.

5.3 Results

Upon feeding the CDAA diet both knockout strains displayed a significantly attenuated weight gain compared to the wild type mice. Moreover, the liver weights of Il4ra $^{-/-}$ strains were lower than those of WT mice fed the CDAA diet. In addition, the intraperitoneal glucose tolerance test revealed no difference in glucose tolerance in Il4ra $^{-/-}$ strains compared their WT controls fed the CDAA diet, as shown in **Fig.16**. H&E stained sections revealed a significant reduction of the NAS score adapted for mice, decreasing from 6.0±0.67 to 4.0±0.9 for Il4ra $^{-/-}$ and 4.0±1.12 for LysM^{cre}IL4Rα$^{-/lox}$ and the histological stage of fibrosis score was 1.0 (mild, perisinusoidal in zone 3) in both Il4ra $^{-/-}$ strains vs a stage of 2.0 in in the WT controls (perisinusoidal and portal/periportal fibrosis with occasional bridging), as shown in **Fig.17**. Moreover, CD68+ foci in liver sections of both Il4ra $^{-/-}$ strains were significantly reduced vs the WT mice fed the CDAA diet (**Fig.18**). Hydroxyproline quantification and Sirius red morphometry confirmed a significant (up to 50%) reduction of collagen accumulation in the knockout vs wildtype animals (**Fig.19**). In wild type mice, steatosis was >66% and macrovesicular, whereas steatosis was reduced to <50%, more concentrated in zone 3 and prominently microvesicular in the IL4Ra knockout mice. Moreover, alpha SMA morphometry indicated a significant reduction of hepatic stellate cell/myofibroblast activation in both IL4Ra-/- mouse lines compare to the WT mice (**Fig.20**). All these data are displayed in the following figures.
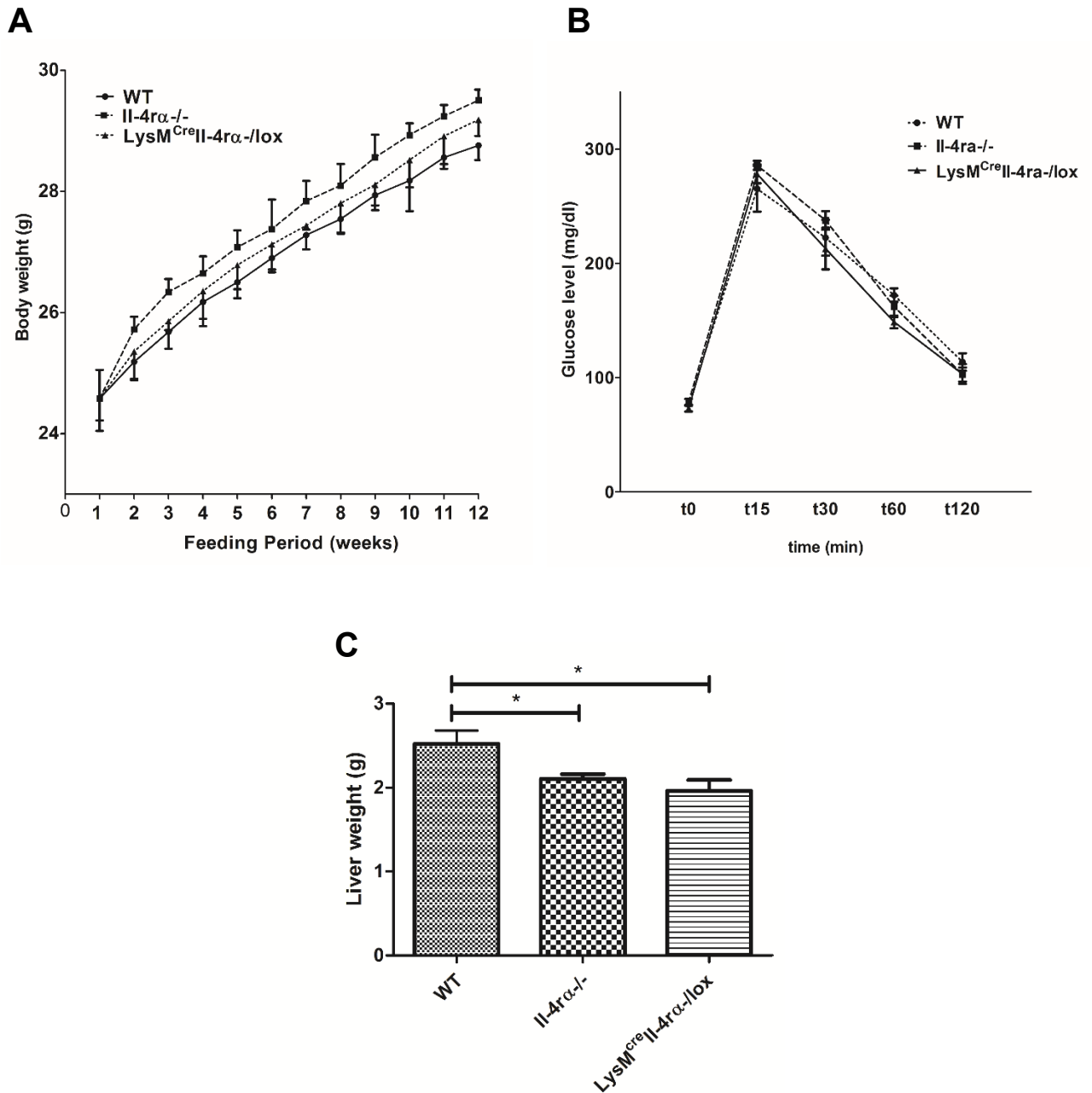
Fig.16 Weight base indices and intra glucose tolerance test. (A) Change in body weight (B) Intraperitoneal glucose tolerance test (IPGTT). (C) Liver weights of CDAA. Comparisons by ANOVA; data are means ± SEM for 7-10 representative sections per mouse and 6-8 mice per group; *p<0.05, **p<0.01, ***p<0.001
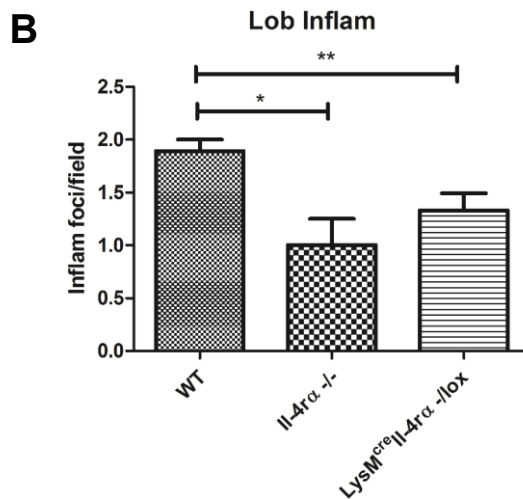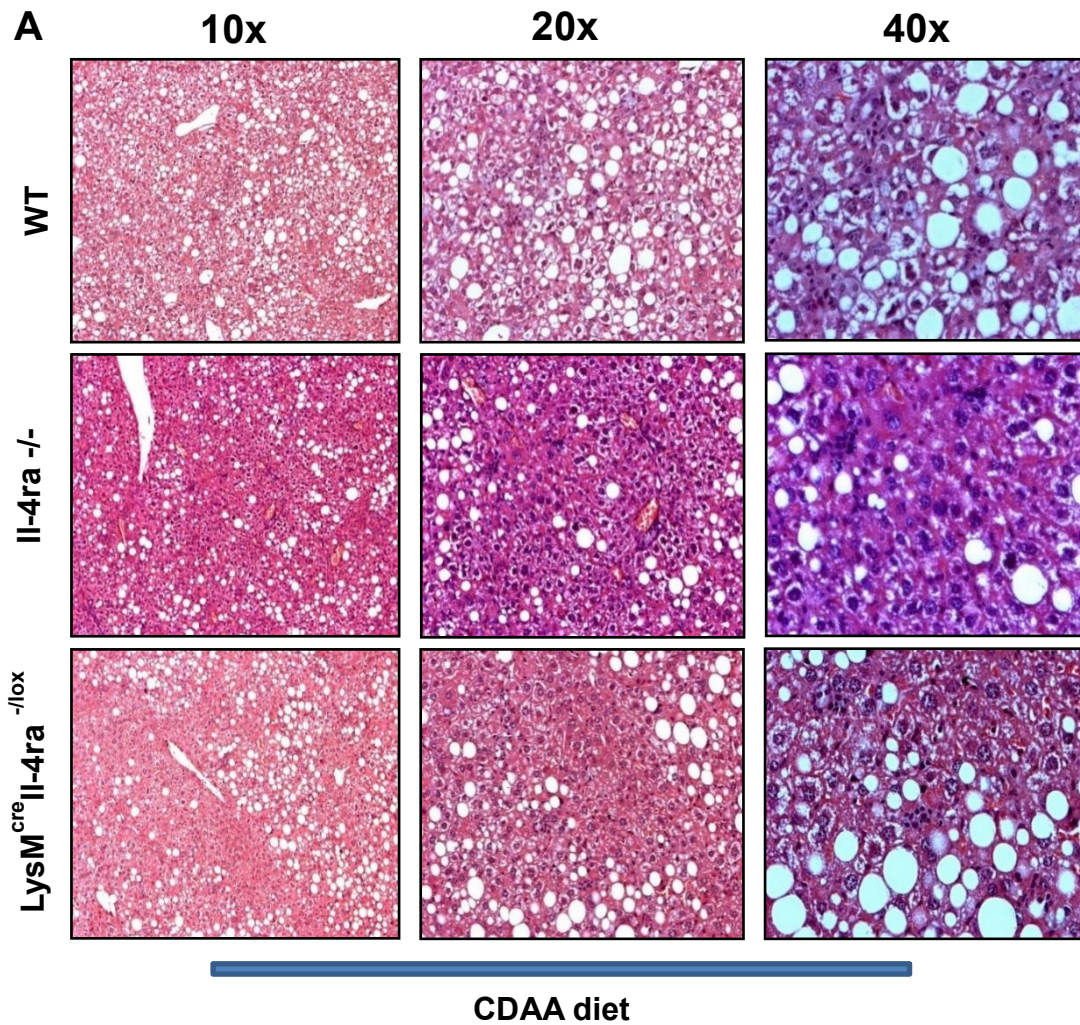
Fig.17 Representative images of H&E stained liver sections morphometrical evaluation (A, B). Scale bar: 50µm. Comparisons by ANOVA; data are means ± SEM for 6-8 representative sections per mouse and 6-8 mice per group; *$p < 0.05$, **$p < 0.01$, ***$p < 0.001$.
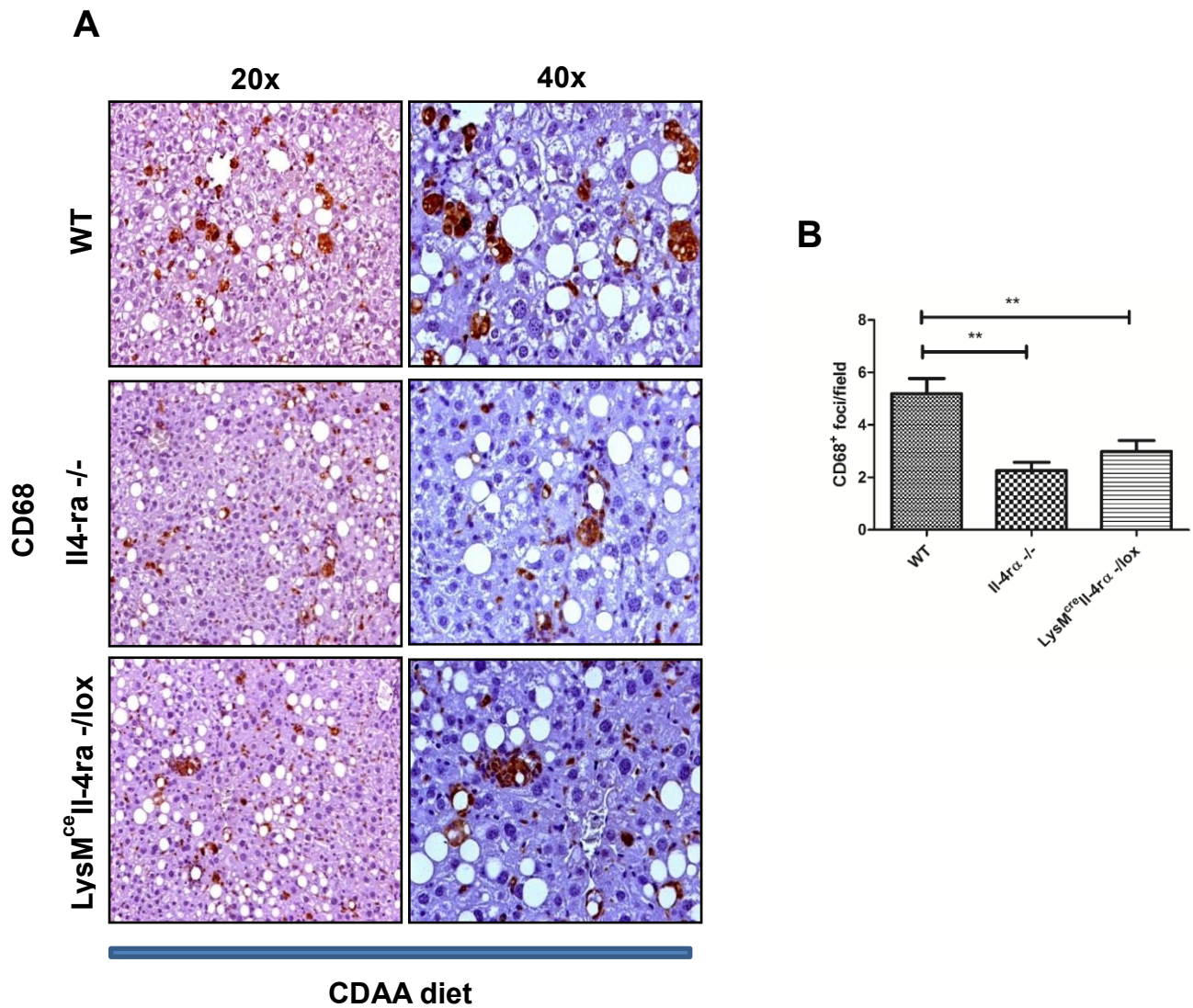
Fig.18 Immunohistochemistry for hepatic expression of CD68⁺. Il4ra-/- strains vs WT controls fed the CDAA. Scale bar: 50µm (A) morphometrical evaluation (B). Comparisons by ANOVA; data are means ± SEM for 6-8 representative sections per mouse and 6-8 mice per group; *p<0.05, **p<0.01, ***p<0.001.
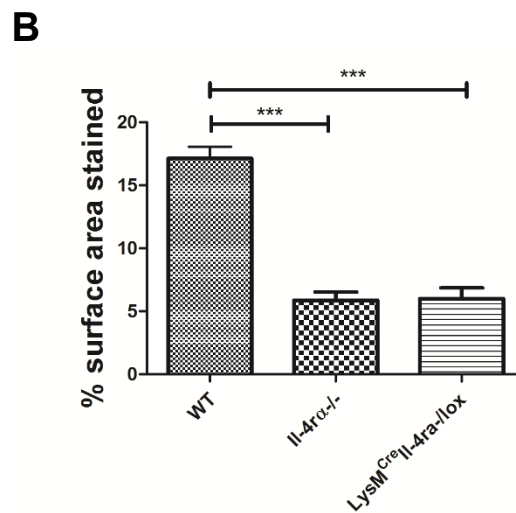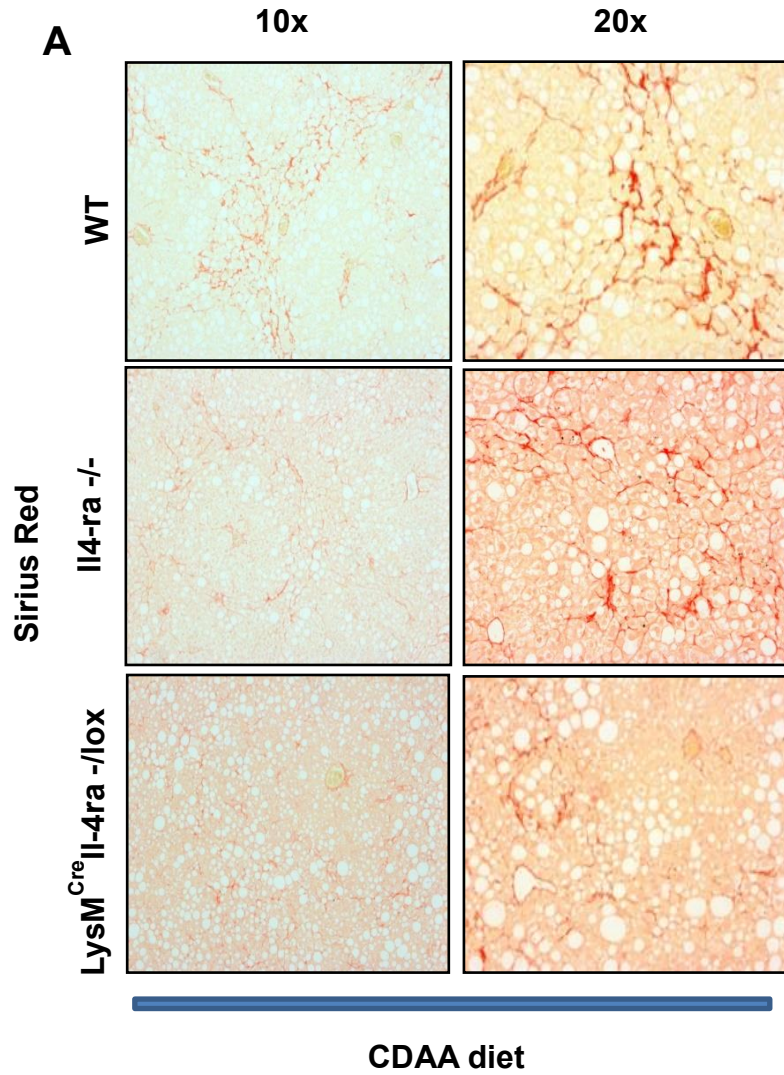
Fig.19 Sirius Red staining of liver sections. Il4ra-/- strains vs WT controls fed the CDAA diets scale bar: 50μm (A) Morphometrical evaluation (B) Ccomparisons by ANOVA; data are means ± SEM for 7-10 representative sections per mouse and 6-8 mice per group; *p<0.05, **p<0.01, ***p<0.001.
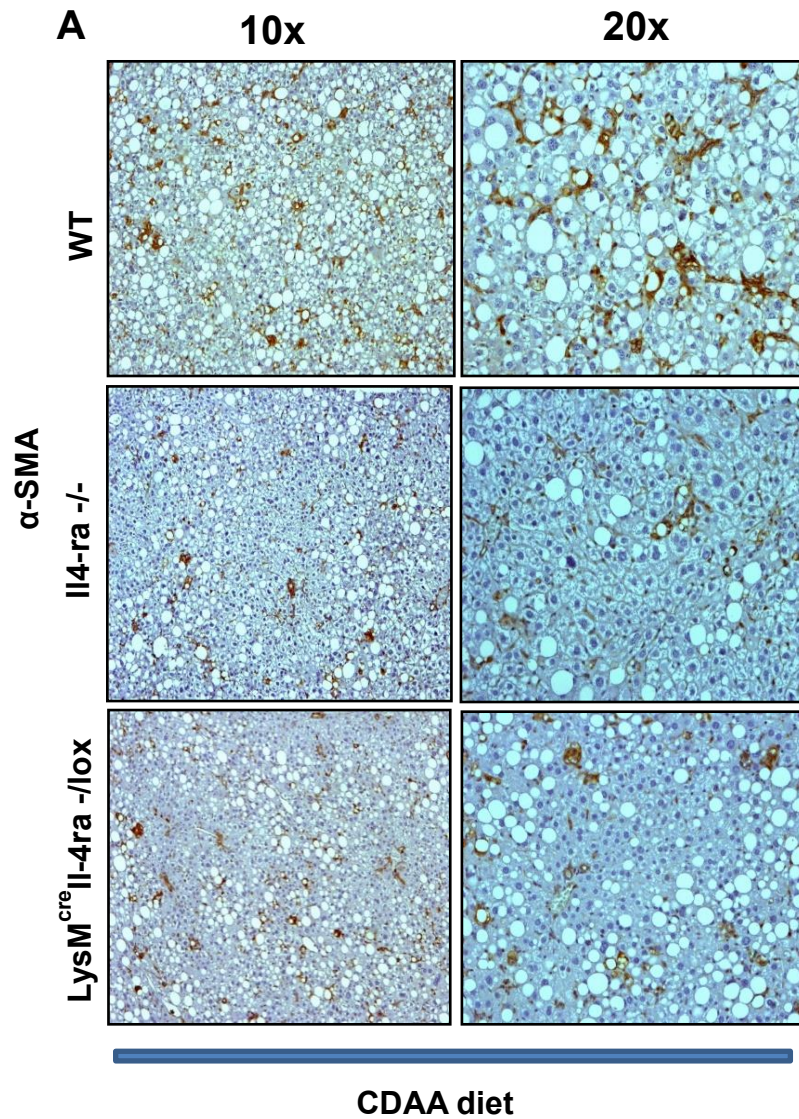
Fig.20. **Immunohistochemistry for alpha-SMA in liver sections.** Il4ra-/- strains vs WT controls fed the CDAA Scale bar 50µm (A). Morphometrical evaluation (B) Comparisons by ANOVA; data are means ± SEM for 5 representative sections per mouse and 6-8 mice per group; *p<0.05, **p<0.01, ***p<0.001.
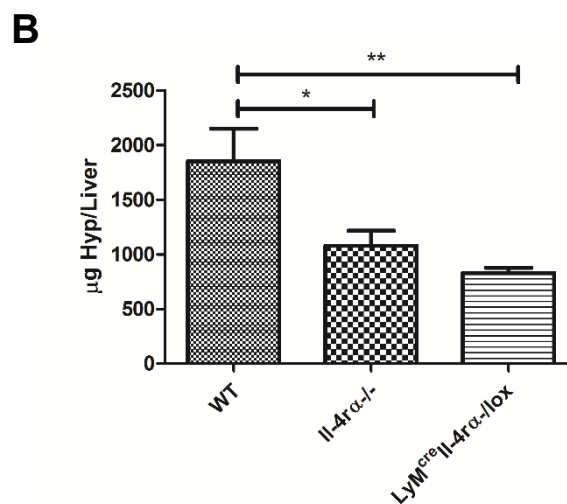
5.4 Conclusions

1. Ablation of the IL4Rα on monocytes-macrophages and in general comparably suppressed steatosis, inflammation and fibrosis in the CDAA model of NASH; 2. IL4Rα receptor mediated targeted therapies are a better therapeutic option than inhibition of IL4 and IL13 cytokines for fibrotic NASH.

6. References

1. Schuppan D, Surabattula R, Wang XY. Determinants of fibrosis progression and regression in NASH. J Hepatol 2018;68:238-250.
2. Kabbany MN, Conjeevaram Selvakumar PK, Watt K, et al. Prevalence of Nonalcoholic Steatohepatitis-Associated Cirrhosis in the United States: An Analysis of National Health and Nutrition Examination Survey Data. Am J Gastroenterol 2017;112:581-587.
3. Vernon G, Baranova A, Younossi ZM. Systematic review: the epidemiology and natural history of non-alcoholic fatty liver disease and non-alcoholic steatohepatitis in adults. Aliment Pharmacol Ther 2011;34:274-85.
4. Minervini MI, Ruppert K, Fontes P, et al. Liver biopsy findings from healthy potential living liver donors: reasons for disqualification, silent diseases and correlation with liver injury tests. J Hepatol 2009;50:501-10.
5. Ryan CK, Johnson LA, Germin BI, et al. One hundred consecutive hepatic biopsies in the workup of living donors for right lobe liver transplantation. Liver Transpl 2002;8:1114-22.
6. Wanless IR, Lentz JS. Fatty liver hepatitis (steatohepatitis) and obesity: an autopsy study with analysis of risk factors. Hepatology 1990;12:1106-10.
7. Kim G-A, Lee HC, Choe J, et al. Association between non-alcoholic fatty liver disease and cancer incidence rate. Journal of Hepatology.
8. Younossi ZM, Koenig AB, Abdelatif D, et al. Global epidemiology of nonalcoholic fatty liver disease-Meta-analytic assessment of prevalence, incidence, and outcomes. Hepatology 2016;64:73-84.
9. Bellentani S, Scaglioni F, Marino M, et al. Epidemiology of non-alcoholic fatty liver disease. Dig Dis 2010;28:155-61.
10. Anstee QM, McPherson S, Day CP. How big a problem is non-alcoholic fatty liver disease? BMJ 2011;343.
11. de Alwis NMW, Day CP. Non-alcoholic fatty liver disease: The mist gradually clears. Journal of Hepatology;48:S104-S112.
12. Sanyal AJ. AGA technical review on nonalcoholic fatty liver disease. Gastroenterology;123:1705-1725.
13. Anstee QM, Daly AK, Day CP. Genetic modifiers of non-alcoholic fatty liver disease progression. Biochim Biophys Acta 2011;1812:1557-66.
14. Iredale JP. Models of liver fibrosis: exploring the dynamic nature of inflammation and repair in a solid organ. J Clin Invest 2007;117:539-48.
15. Winer DA, Winer S, Dranse HJ, et al. Immunologic impact of the intestine in metabolic disease. J Clin Invest 2017;127:33-42.
16. Hardy T, Oakley F, Anstee QM, et al. Nonalcoholic Fatty Liver Disease: Pathogenesis and Disease Spectrum. Annu Rev Pathol 2016;11:451-96.
17. Junker Y, Zeissig S, Kim SJ, et al. Wheat amylase trypsin inhibitors drive intestinal inflammation via activation of toll-like receptor 4. J Exp Med 2012;209:2395-408.
18. Zevallos VF, Raker V, Tenzer S, et al. Nutritional Wheat Amylase-Trypsin Inhibitors Promote Intestinal Inflammation via Activation of Myeloid Cells. Gastroenterology 2016.
19. Wieckowska A, Feldstein AE. Diagnosis of nonalcoholic fatty liver disease: invasive versus noninvasive. Semin Liver Dis 2008;28:386-95.
20. Loomba R, Wolfson T, Ang B, et al. Magnetic resonance elastography predicts advanced fibrosis in patients with nonalcoholic fatty liver disease: a prospective study. Hepatology 2014;60:1920-8.
21. Banerjee R, Pavlides M, Tunnicliffe EM, et al. Multiparametric magnetic resonance for the non-invasive diagnosis of liver disease. J Hepatol 2014;60:69-77.
22. George J, Anstee Q, Ratziu V, et al. NAFLD: The evolving landscape. J Hepatol 2018;68:227-229.

23. Loomba R. Role of imaging-based biomarkers in NAFLD: Recent advances in clinical application and future research directions. J Hepatol 2018;68:296-304.
24. Yeh MM, Brunt EM. Pathological features of fatty liver disease. Gastroenterology 2014;147:754-64.
25. Kleiner DE, Brunt EM, Van Natta M, et al. Design and validation of a histological scoring system for nonalcoholic fatty liver disease. Hepatology 2005;41:1313-21.
26. Lackner C, Gogg-Kamerer M, Zatloukal K, et al. Ballooned hepatocytes in steatohepatitis: the value of keratin immunohistochemistry for diagnosis. J Hepatol 2008;48:821-8.
27. Brunt EM, Kleiner DE, Wilson LA, et al. Portal chronic inflammation in nonalcoholic fatty liver disease (NAFLD): a histologic marker of advanced NAFLD-Clinicopathologic correlations from the nonalcoholic steatohepatitis clinical research network. Hepatology 2009;49:809-20.
28. Brunt EM, Janney CG, Di Bisceglie AM, et al. Nonalcoholic steatohepatitis: a proposal for grading and staging the histological lesions. Am J Gastroenterol 1999;94:2467-74.
29. Ibrahim SH, Hirsova P, Malhi H, et al. Animal Models of Nonalcoholic Steatohepatitis: Eat, Delete, and Inflame. Dig Dis Sci 2016;61:1325-36.
30. Geoff Farrel JMS, Isabelle Lechercq, Mathhew M. Yeh, Robert Goldin, Narci Teoh, Detlef Schuppan. Mouse Models of Non alcoholic steatohepatitis. Hepatology 2018;Accepted.
31. Mayer J, Bates MW, Dickie MM. Hereditary diabetes in genetically obese mice. Science 1951;113:746-7.
32. Leclercq IA, Field J, Farrell GC. Leptin-specific mechanisms for impaired liver regeneration in ob/ob mice after toxic injury. Gastroenterology 2003;124:1451-64.
33. Chalasani N, Crabb DW, Cummings OW, et al. Does leptin play a role in the pathogenesis of human nonalcoholic steatohepatitis? Am J Gastroenterol 2003;98:2771-6.
34. Chen H, Charlat O, Tartaglia LA, et al. Evidence that the diabetes gene encodes the leptin receptor: identification of a mutation in the leptin receptor gene in db/db mice. Cell 1996;84:491-5.
35. Santhekadur PK, Kumar DP, Sanyal AJ. Preclinical models of non-alcoholic fatty liver disease. J Hepatol 2018;68:230-237.
36. Tetri LH, Basaranoglu M, Brunt EM, et al. Severe NAFLD with hepatic necroinflammatory changes in mice fed trans fats and a high-fructose corn syrup equivalent. Am J Physiol Gastrointest Liver Physiol 2008;295:G987-95.
37. Matsuzawa N, Takamura T, Kurita S, et al. Lipid-induced oxidative stress causes steatohepatitis in mice fed an atherogenic diet. Hepatology 2007;46:1392-403.
38. Van Rooyen DM, Larter CZ, Haigh WG, et al. Hepatic free cholesterol accumulates in obese, diabetic mice and causes nonalcoholic steatohepatitis. Gastroenterology 2011;141:1393-403, 1403 e1-5.
39. Gao D, Wei C, Chen L, et al. Oxidative DNA damage and DNA repair enzyme expression are inversely related in murine models of fatty liver disease. Am J Physiol Gastrointest Liver Physiol 2004;287:G1070-7.
40. Friedman SL, Sheppard D, Duffield JS, et al. Therapy for fibrotic diseases: nearing the starting line. Sci Transl Med 2013;5:167sr1.
41. Talwalkar JA, Lindor KD. Primary sclerosing cholangitis. Inflamm Bowel Dis 2005;11:62-72.
42. Pinzani M, Luong TV. Pathogenesis of biliary fibrosis. Biochim Biophys Acta Mol Basis Dis 2018;1864:1279-1283.
43. Popov Y, Patsenker E, Fickert P, et al. Mdr2 (Abcb4)-/- mice spontaneously develop severe biliary fibrosis via massive dysregulation of pro- and antifibrogenic genes. J Hepatol 2005;43:1045-54.
44. Roskams TA, Theise ND, Balabaud C, et al. Nomenclature of the finer branches of the biliary tree: canals, ductules, and ductular reactions in human livers. Hepatology 2004;39:1739-45.
45. Trauner M, Fickert P, Wagner M. MDR3 (ABCB4) defects: a paradigm for the genetics of adult cholestatic syndromes. Semin Liver Dis 2007;27:77-98.

46. Fickert P, Fuchsbichler A, Wagner M, et al. Regurgitation of bile acids from leaky bile ducts causes sclerosing cholangitis in Mdr2 (Abcb4) knockout mice. Gastroenterology 2004;127:261-74.
47. Lammert F, Wang DQ, Hillebrandt S, et al. Spontaneous cholecysto- and hepatolithiasis in Mdr2-/- mice: a model for low phospholipid-associated cholelithiasis. Hepatology 2004;39:117-28.
48. Smit JJ, Schinkel AH, Oude Elferink RP, et al. Homozygous disruption of the murine mdr2 P-glycoprotein gene leads to a complete absence of phospholipid from bile and to liver disease. Cell 1993;75:451-62.
49. Davit-Spraul A, Gonzales E, Baussan C, et al. Progressive familial intrahepatic cholestasis. Orphanet J Rare Dis 2009;4:1.
50. Yang L, Seki E. Toll-like receptors in liver fibrosis: cellular crosstalk and mechanisms. Front Physiol 2012;3:138.
51. Seki E, De Minicis S, Osterreicher CH, et al. TLR4 enhances TGF-beta signaling and hepatic fibrosis. Nat Med 2007;13:1324-32.
52. Yan C, Li B, Fan F, et al. The roles of Toll-like receptor 4 in the pathogenesis of pathogen-associated biliary fibrosis caused by Clonorchis sinensis. Sci Rep 2017;7:3909.
53. Zevallos VF, Raker V, Tenzer S, et al. Nutritional Wheat Amylase-Trypsin Inhibitors Promote Intestinal Inflammation via Activation of Myeloid Cells. Gastroenterology 2017;152:1100-1113 e12.
54. Wiest R, Albillos A, Trauner M, et al. Targeting the gut-liver axis in liver disease. J Hepatol 2017;67:1084-1103.
55. Compare D, Coccoli P, Rocco A, et al. Gut--liver axis: the impact of gut microbiota on non alcoholic fatty liver disease. Nutr Metab Cardiovasc Dis 2012;22:471-6.
56. Racanelli V, Rehermann B. The liver as an immunological organ. Hepatology 2006;43:S54-62.
57. Sheth K, Bankey P. The liver as an immune organ. Curr Opin Crit Care 2001;7:99-104.
58. Jin X, Yu CH, Lv GC, et al. Increased intestinal permeability in pathogenesis and progress of nonalcoholic steatohepatitis in rats. World J Gastroenterol 2007;13:1732-6.
59. Kirpich IA, Marsano LS, McClain CJ. Gut-liver axis, nutrition, and non-alcoholic fatty liver disease. Clin Biochem 2015;48:923-30.
60. Alisi A, Carsetti R, Nobili V. Pathogen- or damage-associated molecular patterns during nonalcoholic fatty liver disease development. Hepatology 2011;54:1500-2.
61. Alisi A, Manco M, Devito R, et al. Endotoxin and plasminogen activator inhibitor-1 serum levels associated with nonalcoholic steatohepatitis in children. J Pediatr Gastroenterol Nutr 2010;50:645-9.
62. Rahman K, Desai C, Iyer SS, et al. Loss of Junctional Adhesion Molecule A Promotes Severe Steatohepatitis in Mice on a Diet High in Saturated Fat, Fructose, and Cholesterol. Gastroenterology 2016;151:733-746 e12.
63. Altenbach SB, Vensel WH, Dupont FM. The spectrum of low molecular weight alpha-amylase/protease inhibitor genes expressed in the US bread wheat cultivar Butte 86. BMC Res Notes 2011;4:242.
64. Oda Y, Matsunaga T, Fukuyama K, et al. Tertiary and quaternary structures of 0.19 alpha-amylase inhibitor from wheat kernel determined by X-ray analysis at 2.06 A resolution. Biochemistry 1997;36:13503-11.
65. Tatham AS, Shewry PR. Allergens to wheat and related cereals. Clin Exp Allergy 2008;38:1712-26.
66. Franco OL, Rigden DJ, Melo FR, et al. Plant alpha-amylase inhibitors and their interaction with insect alpha-amylases. Eur J Biochem 2002;269:397-412.
67. Choudhury A, Maeda K, Murayama R, et al. Character of a wheat amylase inhibitor preparation and effects on fasting human pancreaticobiliary secretions and hormones. Gastroenterology 1996;111:1313-20.

68.	Dupont FM, Vensel WH, Tanaka CK, et al. Deciphering the complexities of the wheat flour proteome using quantitative two-dimensional electrophoresis, three proteases and tandem mass spectrometry. Proteome Sci 2011;9:10.

69.	Tilg H, Koch R, Moschen AR. Proinflammatory wheat attacks on the intestine: alpha-amylase trypsin inhibitors as new players. Gastroenterology 2013;144:1561-3; discussion 1563-4.

70.	Schuppan D, Zevallos V. Wheat amylase trypsin inhibitors as nutritional activators of innate immunity. Dig Dis 2015;33:260-3.

71.	Bellinghausen I, Weigmann B, Zevallos V, et al. Wheat amylase-trypsin inhibitors exacerbate intestinal and airway allergic immune responses in humanized mice. J Allergy Clin Immunol 2018.

72.	Zevallos VF, Raker VK, Maxeiner J, et al. Dietary wheat amylase trypsin inhibitors exacerbate murine allergic airway inflammation. Eur J Nutr 2018.

73.	Abdul-Rahman NA, Azman RR, Kumar G. Adult female with acute renal failure and weight loss. Saudi Med J 2016;37:584-6.

74.	Wang X, Hausding M, Weng SY, et al. Gliptins Suppress Inflammatory Macrophage Activation to Mitigate Inflammation, Fibrosis, Oxidative Stress, and Vascular Dysfunction in Models of Nonalcoholic Steatohepatitis and Liver Fibrosis. Antioxid Redox Signal 2018;28:87-109.

75.	Popov Y, Patsenker E, Bauer M, et al. Halofuginone induces matrix metalloproteinases in rat hepatic stellate cells via activation of p38 and NFkappaB. J Biol Chem 2006;281:15090-8.

76.	Murano I, Barbatelli G, Parisani V, et al. Dead adipocytes, detected as crown-like structures, are prevalent in visceral fat depots of genetically obese mice. J Lipid Res 2008;49:1562-8.

77.	Charmet G. Wheat domestication: lessons for the future. C R Biol 2011;334:212-20.

78.	Shewry PR, Halford NG, Lafiandra D. Genetics of wheat gluten proteins. Adv Genet 2003;49:111-84.

79.	Medzhitov R. Recognition of microorganisms and activation of the immune response. Nature 2007;449:819-26.

80.	Mokhtari Z, Gibson DL, Hekmatdoost A. Nonalcoholic Fatty Liver Disease, the Gut Microbiome, and Diet. Adv Nutr 2017;8:240-252.

81.	Fasano A, Sapone A, Zevallos V, et al. Nonceliac gluten sensitivity. Gastroenterology 2015;148:1195-204.

82.	Schuppan D, Pickert G, Ashfaq-Khan M, et al. Non-celiac wheat sensitivity: differential diagnosis, triggers and implications. Best Pract Res Clin Gastroenterol 2015;29:469-76.

83.	Saltiel AR, Olefsky JM. Inflammatory mechanisms linking obesity and metabolic disease. J Clin Invest 2017;127:1-4.

84.	Corey KE, Kaplan LM. Obesity and liver disease: the epidemic of the twenty-first century. Clin Liver Dis 2014;18:1-18.

85.	Stergios AP, Jannis K, Christos Z. Nonalcoholic Fatty Liver Disease: The Pathogenetic Roles of Insulin Resistance and Adipocytokines. Current Molecular Medicine 2009;9:299-314.

86.	Li L, Liu DW, Yan HY, et al. Obesity is an independent risk factor for non-alcoholic fatty liver disease: evidence from a meta-analysis of 21 cohort studies. Obesity Reviews 2016;17:510-519.

87.	Anstee QM, Targher G, Day CP. Progression of NAFLD to diabetes mellitus, cardiovascular disease or cirrhosis. Nat Rev Gastroenterol Hepatol 2013;10:330-44.

88.	Kim CH, Younossi ZM. Nonalcoholic fatty liver disease: a manifestation of the metabolic syndrome. Cleve Clin J Med 2008;75:721-8.

89.	Jumpertz R, Le DS, Turnbaugh PJ, et al. Energy-balance studies reveal associations between gut microbes, caloric load, and nutrient absorption in humans. Am J Clin Nutr 2011;94:58-65.

90.	Scarpellini E, Lupo M, Iegri C, et al. Intestinal permeability in non-alcoholic fatty liver disease: the gut-liver axis. Rev Recent Clin Trials 2014;9:141-7.

91.	Ghoshal S, Witta J, Zhong J, et al. Chylomicrons promote intestinal absorption of lipopolysaccharides. J Lipid Res 2009;50:90-7.

92. Wellen KE, Hotamisligil GS. Obesity-induced inflammatory changes in adipose tissue. J Clin Invest 2003;112:1785-8.

93. Lumeng CN, Bodzin JL, Saltiel AR. Obesity induces a phenotypic switch in adipose tissue macrophage polarization. J Clin Invest 2007;117:175-84.

94. McLaughlin T, Ackerman SE, Shen L, et al. Role of innate and adaptive immunity in obesity-associated metabolic disease. J Clin Invest 2017;127:5-13.

95. Duval C, Thissen U, Keshtkar S, et al. Adipose tissue dysfunction signals progression of hepatic steatosis towards nonalcoholic steatohepatitis in C57BL/6 mice. Diabetes 2010;59:3181-91.

96. Cinti S, Mitchell G, Barbatelli G, et al. Adipocyte death defines macrophage localization and function in adipose tissue of obese mice and humans. J Lipid Res 2005;46:2347-55.

97. Strissel KJ, Stancheva Z, Miyoshi H, et al. Adipocyte death, adipose tissue remodeling, and obesity complications. Diabetes 2007;56:2910-8.

98. du Plessis J, van Pelt J, Korf H, et al. Association of Adipose Tissue Inflammation With Histologic Severity of Nonalcoholic Fatty Liver Disease. Gastroenterology 2015;149:635-48 e14.

99. Tilg H, Moschen AR. Evolution of inflammation in nonalcoholic fatty liver disease: the multiple parallel hits hypothesis. Hepatology 2010;52:1836-46.

100. Park EJ, Lee JH, Yu GY, et al. Dietary and genetic obesity promote liver inflammation and tumorigenesis by enhancing IL-6 and TNF expression. Cell 2010;140:197-208.

101. Tosello-Trampont AC, Landes SG, Nguyen V, et al. Kuppfer cells trigger nonalcoholic steatohepatitis development in diet-induced mouse model through tumor necrosis factor-alpha production. J Biol Chem 2012;287:40161-72.

102. Nakagawa H, Umemura A, Taniguchi K, et al. ER stress cooperates with hypernutrition to trigger TNF-dependent spontaneous HCC development. Cancer Cell 2014;26:331-343.

103. Dixon LJ, Flask CA, Papouchado BG, et al. Caspase-1 as a central regulator of high fat diet-induced non-alcoholic steatohepatitis. PLoS One 2013;8:e56100.

104. Csak T, Ganz M, Pespisa J, et al. Fatty acid and endotoxin activate inflammasomes in mouse hepatocytes that release danger signals to stimulate immune cells. Hepatology 2011;54:133-44.

105. Hendrikx T, Bieghs V, Walenbergh SM, et al. Macrophage specific caspase-1/11 deficiency protects against cholesterol crystallization and hepatic inflammation in hyperlipidemic mice. PLoS One 2013;8:e78792.

106. Ye D, Li FY, Lam KS, et al. Toll-like receptor-4 mediates obesity-induced non-alcoholic steatohepatitis through activation of X-box binding protein-1 in mice. Gut 2012;61:1058-67.

107. Wigg AJ, Roberts-Thomson IC, Dymock RB, et al. The role of small intestinal bacterial overgrowth, intestinal permeability, endotoxaemia, and tumour necrosis factor alpha in the pathogenesis of non-alcoholic steatohepatitis. Gut 2001;48:206-11.

108. Miele L, Valenza V, La Torre G, et al. Increased intestinal permeability and tight junction alterations in nonalcoholic fatty liver disease. Hepatology 2009;49:1877-87.

109. Imajo K, Fujita K, Yoneda M, et al. Hyperresponsivity to low-dose endotoxin during progression to nonalcoholic steatohepatitis is regulated by leptin-mediated signaling. Cell Metab 2012;16:44-54.

110. Zwolak A, Szuster-Ciesielska A, Daniluk J, et al. Hyperreactivity of Blood Leukocytes in Patients with NAFLD to Ex Vivo Lipopolysaccharide Treatment Is Modulated by Metformin and Phosphatidylcholine but Not by Alpha Ketoglutarate. PLoS One 2015;10:e0143851.

111. Narayanan S, Surette FA, Hahn YS. The Immune Landscape in Nonalcoholic Steatohepatitis. Immune Netw 2016;16:147-58.

112. Anstee QM, McPherson S, Day CP. How big a problem is non-alcoholic fatty liver disease? BMJ 2011;343:d3897.

113. Rajapaksha IG, Mak KY, Huang P, et al. The small molecule drug diminazene aceturate inhibits liver injury and biliary fibrosis in mice. Sci Rep 2018;8:10175.

114. Schuppan D, Ashfaq-Khan M, Yang AT, et al. Liver fibrosis: Direct antifibrotic agents and targeted therapies. Matrix Biol 2018;68-69:435-451.

115. Krenkel O, Tacke F. Liver macrophages in tissue homeostasis and disease. Nat Rev Immunol 2017;17:306-321.

116. Karlmark KR, Weiskirchen R, Zimmermann HW, et al. Hepatic recruitment of the inflammatory Gr1+ monocyte subset upon liver injury promotes hepatic fibrosis. Hepatology 2009;50:261-74.

117. Marra F, DeFranco R, Grappone C, et al. Increased expression of monocyte chemotactic protein-1 during active hepatic fibrogenesis: correlation with monocyte infiltration. Am J Pathol 1998;152:423-30.

118. Shimizu Y, Murata H, Kashii Y, et al. CC-chemokine receptor 6 and its ligand macrophage inflammatory protein 3alpha might be involved in the amplification of local necroinflammatory response in the liver. Hepatology 2001;34:311-9.

119. Ju C, Tacke F. Hepatic macrophages in homeostasis and liver diseases: from pathogenesis to novel therapeutic strategies. Cell Mol Immunol 2016;13:316-27.

120. Gieseck RL, 3rd, Wilson MS, Wynn TA. Type 2 immunity in tissue repair and fibrosis. Nat Rev Immunol 2018;18:62-76.

121. Hart KM, Fabre T, Sciurba JC, et al. Type 2 immunity is protective in metabolic disease but exacerbates NAFLD collaboratively with TGF-beta. Sci Transl Med 2017;9.

122. Izuhara K, Arima K, Yasunaga S. IL-4 and IL-13: their pathological roles in allergic diseases and their potential in developing new therapies. Curr Drug Targets Inflamm Allergy 2002;1:263-9.

123. Fish SC, Donaldson DD, Goldman SJ, et al. IgE generation and mast cell effector function in mice deficient in IL-4 and IL-13. J Immunol 2005;174:7716-24.

124. Grunig G, Warnock M, Wakil AE, et al. Requirement for IL-13 independently of IL-4 in experimental asthma. Science 1998;282:2261-3.

125. Chatila TA. Interleukin-4 receptor signaling pathways in asthma pathogenesis. Trends Mol Med 2004;10:493-9.

126. Wills-Karp M, Finkelman FD. Untangling the complex web of IL-4- and IL-13-mediated signaling pathways. Sci Signal 2008;1:pe55.

127. Weng SY, Wang X, Vijayan S, et al. IL-4 Receptor Alpha Signaling through Macrophages Differentially Regulates Liver Fibrosis Progression and Reversal. EBioMedicine 2018;29:92-103.